ECMWF COPERNICUS REPORT

Copernicus Atmosphere Monitoring Service

Observations characterization and validation methods document

Issued by: KNMI

Date: 5 October 2017

Ref: CAMS84_2015SC2_D84.8.1.1-2017_observations_v2

IMPLEMENTED BY ECMWF

Observations characterisation and validation methods document

AUTHORS:
S. Basart (BSC), A. Benedictow (MetNo), A.-M. Blechschmidt (IUP-UB), S. Chabrillat (BIRA-IASB), Y. Christophe (BIRA-IASB), H. Clark (CNRS-LA), E. Cuevas (AEMET), H. Flentje (DWD), K. M. Hansen (AU), J. Kapsomenakis (AA), B. Langerock (BIRA-IASB), K. Petersen (MPG), M. Ramonet (CEA-LSCE), A. Richter (IUP-UB), M. Schulz (MetNo), A. Wagner (MPG), T. Warneke (UBC), C. Zerefos (AA)

EDITORS:
J. Douros (KNMI), H.J. Eskes (KNMI)

REPORT OF THE COPERNICUS ATMOSPHERE MONITORING SERVICE, VALIDATION SUBPROJECT (CAMS-84).

CITATION:
J. Douros, S. Basart, A. Benedictow, A.-M. Blechschmidt, S. Chabrillat, Y. Christophe, H. Clark, E. Cuevas, H.J. Eskes, H. Flentje, K. M. Hansen, J. Kapsomenakis, B. Langerock, K. Petersen, M. Ramonet, A. Richter, M. Schulz, A. Wagner, T. Warneke, C. Zerefos, Observations characterisation and validation methods document, Copernicus Atmosphere Monitoring Service (CAMS) report, CAMS84_2015SC2_D.84.8.1.1-2017_observations_v2.pdf, October 2017.

STATUS:
Version 2, final

DATE:
5 October 2017

REF:
CAMS84_2015SC2_D84.8.1.1-2017_observations_v2

Executive Summary

The Copernicus Atmosphere Monitoring Service (http://atmosphere.copernicus.eu, CAMS) is a component of the European Earth Observation program Copernicus. CAMS is providing operational forecasts, analyses and reanalyses on the global and European scale of the composition of the atmosphere (reactive gases, greenhouse gases, aerosols).

CAMS-84 is a sub-project of CAMS, dealing with the validation of the services. CAMS-84 provides 3-monthly updates of validation reports for the global and regional services. The validation is based on a large number of observations and measurement techniques, including surface in-situ, surface remote sensing, observations by airplanes, balloon sounding, observations from ships and satellite observations. The three monthly cycle of the validation reports adds constraints on the availability of the observations, which should be roughly within one month after sensing.

This document serves as a reference for the validation reports, in order to provide the traceability for the independent observations used in the validation work. The two main aspects discussed are:

1. A description of the observations used, including the list of contributing stations, observation networks, measurement techniques, QA procedures, and error estimates.
2. A description of the methods to compare these observations with the CAMS modelling and assimilation products.

The focus of this document is on the evaluation of the real-time global service for reactive trace gases, aerosols, and greenhouse gases. Observations used for the reanalysis will be distinguished from observations used for the quarterly reports, but are not yet discussed in this version 2 of the document.

Version 1 of this document was published on the CAMS website in April 2016.

Table of Contents

1 Introduction

In the sections of this document the individual datasets used for the validation will be discussed one by one. The sections will provide information on the datasets and the way these observations are processed and used for the validation of the CAMS services. A list of relevant references is provided, as well as acknowledgments for the data providers.

Table 1.1 (from Eskes et al., 2015) provides an overview of the trace gas species and aerosol quantities relevant for the real-time global atmospheric composition service. Shown are the data sets assimilated (second column) and the data sets used for validation (third column). Normal text indicates that substantial data are available to either constrain the species in the analysis, or substantial data are available to assess the quality of the analysis. Italic text indicates that measurements are available, but that the impact on the analysis is not very strong or indirect (second column), or that only certain aspects are validated (third column).

An overview of the estimated measurement uncertainties and the temporal and spatial properties of the observations are provided in Table 1.2 (taken from Eskes et al., 2015). Non-satellite data is listed in the first box, satellite data in the second.

Table 1.1. Observations used in the assimilation and validation activities of MACC (CAMS), ordered by species.

Species, vertical range	Assimilation	Validation
Aerosol, optical properties	MODIS Aqua/Terra AOD	AOD, Ångström: AERONET, GAW, Skynet, MISR, OMI, lidar
O_3, stratosphere	MLS, GOME-2A, GOME-2B, OMI, SBUV-2	Sonde, lidar, MWR, FTIR, OSIRIS, OMPS, BASCOE and MSR analyses
O_3, UT/LS	*Indirectly constrained by limb and nadir sounders*	IAGOS, sonde
O_3, free troposphere	*Indirectly constrained by limb and nadir sounders*	IAGOS, sonde
O_3, PBL/surface	–	WMO/GAW and NOAA/ESRL surface ozone, IAGOS
CO, UT/LS	–	IAGOS
CO, free troposphere	IASI, MOPITT	IAGOS, MOPITT, IASI
CO, PBL/surface	*Indirectly constrained by satellite IR sounders*	WMO/GAW and NOAA/ESRL surface ozone, IAGOS
NO_2, troposphere	*OMI, partly constrained due to short lifetime*	SCIAMACHY, GOME-2, UV–VIS DOAS
HCHO	–	SCIAMACHY, GOME-2, UV–VIS DOAS
SO_2	*OMI (Individual volcanic eruptions and strong sources)*	–
Stratosphere, other than O_3	–	*SCIAMACHY, GOME-2 (NO_2 column only)*

Table 1.2. Uncertainties and properties of the datasets used for validation.

Data set name	Temporal/spatial frequency	Typical uncertainty
Ozone sondes	38 stations worldwide	uncertainty $<7\,\%$ for 20–30 km altitudes, $\approx 15\,\%$ in the troposphere
GAW O_3	13 stations with NRT data	≈ 5 ppb for NRT, 1 ppb for validated data
NOAA/ESRL O_3	15 stations globally, 3-hourly	1 ppb
GAW CO	11 stations with NRT data	≈ 10 ppb for NRT, 2–5 ppb for validated data
IAGOS O_3	six commercial aircraft	2 ppb $\pm 2\,\%$ for O_3 (Nedelec et al., 2015)
IAGOS CO	six commercial aircraft	5 ppb $\pm\,5\,\%$ for CO (Nedelec et al., 2015)
Aeronet AOD	15 min observations averaged to daily mean, ≈ 400 ground sites	0.01 on AOD
Ceilometer	surface network in Germany	$\pm 50\,\%$ on aerosol extinction coefficients (Wiegner and Geiß, 2012)
NDACC FTIR O_3	daily measurements	3 % on stratospheric column
MOPITT CO	22 km × 22 km footprint, global coverage every 3 days	$<10\,\%$
IASI CO	12 km footprint diameter, near-global coverage 2 × per day	$<10\,\%$
GOME-2 NO_2, HCHO columns	footprint 40 km × 80 km, near-global coverage in 1 day	systematic uncertainties ≈ 20–$30\,\%$ in polluted regions
SCIAMACHY NO_2, HCHO	footprint 30 km × 60 km, global coverage in 6 days	systematic uncertainties ≈ 20–$30\,\%$ in polluted regions
ACE-FTS, O_3, v3	12 profiles/day	5 % (Dupuy et al., 2009)
OSIRIS, O_3, v5	200 profiles/day	5 % (Adams et al., 2014)
OMPS-LP, O_3, v2	6000 profiles/day	up to 10 % (Kramarova et al., 2014)

The description of the observations covers the following aspects:

1. Introduction to the instruments & observation network providing the data;
2. List of stations;
3. List of measurements (species, aerosol properties);
4. Specification of the instruments;
5. Specification of the QA/QC procedures and processing;
6. Error estimates for the observations;
7. Analysis of the location of individual stations, representativity errors, possibly selection criteria to discard stations;
8. An appropriate list of references;
9. Acknowledgements

The description of the validation methodology covers the following aspects:

1. Units of quantity, list the unit conversion operations;
2. Specification of averaging over regions, time;
3. Description how observations and models are compared, including e.g. averaging kernels and regridding;

4. Use of error bars & uncertainty propagation (how are individual observation errors translated to comparison errors);
5. A-posteriori discarding of some stations (if applicable) or checks on outliers.

2 Ozonesonde observations

Ozonesondes are small, lightweight balloon borne instruments, developed for measuring the vertical distribution of atmospheric ozone up to an altitude of about 30-35 km and interfaced to a standard meteorological radiosonde for data transmission to the ground station (e.g. Smit, 2002). There are different sonde types in use, the most common ones are i.e. Brewer-Mast (Brewer and Milford, 1960), electrochemical concentration cell (ECC) (Komhyr 1969), and the carbon iodine cell (Kobayashi and Toyama, 1966), each having its one specific design but all the sensors utilize the principle of the fast reaction of ozone and iodide within an electrochemical cell (Smit, 2002).

Ozonesonde measurements are regularly downloaded from the Norwegian Institute for Air Research (NILU), the World Ozone and Ultraviolet Radiation Data Centre (WOUDC), the Network for the Detection of Atmospheric Composition Change (NDACC) and the Southern Hemisphere ADditional OZonesondes (SHADOZ) databases.

The NILU database is a near-real-time service to collect ozonesonde data of registered stations (mostly located in Europe) within a few minutes after a complete sounding. These files are then read and checked for errors (Smit 2013).

The WOUDC database follows the objectives of the GAW quality assurance system, which ensures that the data deposited in the database are consistent, meet GAW quality objectives and contain a comprehensive description of methodology (Smit 2013). The system involves quality assurance, science activity and calibration centres that ensure the quality of observations through adherence to measurement guidelines established by the Scientific Advisory Groups and through calibrations that are traceable to World Calibration Standards.

The SHADOZ and NDACC ozonesonde stations, which largely overlap with the GAW network, follow the same quality assurance routines as in GAW (Staehelin 2008, Smit 2013).

The gross of soundings are performed with ECC sondes, except at Hohenpeissenberg in Germany (Brewer Mast) and at Japanese stations (carbon iodine sensor). The sondes have a precision of 3-5% (~10% in the troposphere for Brewer Mast) and an accuracy of 5-10% for the free troposphere and the stratosphere. Larger accuracies (up to 18%) may occur in altitudes above 28 km. For further detail see J. T. Deshler et al. (2008) and H.G.J. Smit et al (2007, 2013).

In our validation routines, extra format checks ensure that in case the measurement is of non-standard format, the file is rejected.

For the validation, the sonde profiles are compared to the model data closest in time. The gridded model data are linearly interpolated to the latitude and longitude of the stations' location and converted into partial pressure. In the vertical, the ozone sonde data are resampled at the altitude closest to the model level. The horizontal drift during ascend of the sonde is considered negligible in comparison with the global model resolution. For all individual launches the differences between observation and model are calculated and aggregated to monthly means for each station and region (Arctic, Antarctica, Northern midlatitudes, Southern midlatitudes, Tropics) over specific altitude ranges, namely free troposphere and stratosphere. Here, the free troposphere is defined as the

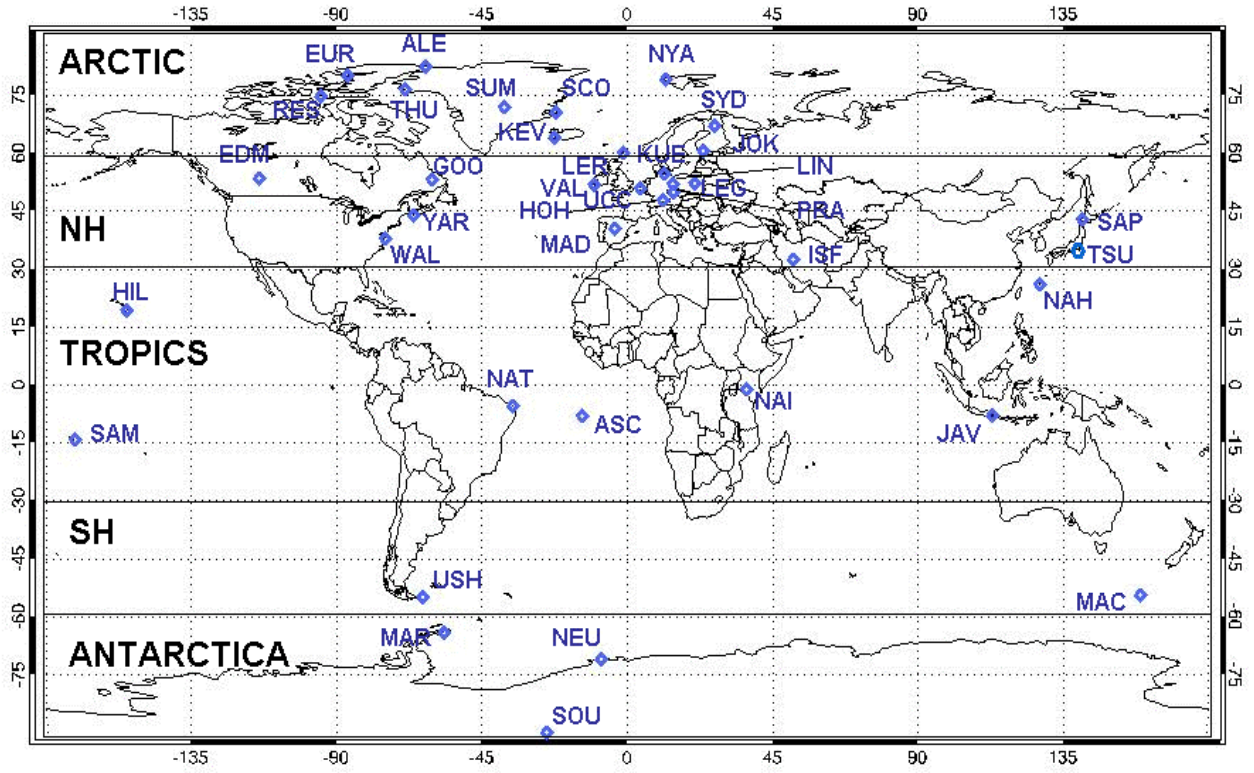

Figure 2.1: Location of the ozone sounding stations and their attribution to the different stratospheric regions

altitude region between 750 and 200 hPa in the tropics and between 750 and 300 hPa elsewhere. The stratosphere is defined as the altitude region between 60 and 10 hPa in the tropics and between 90 and 10 hPa elsewhere.

Profile plots for each month display mean model profiles in comparison with mean monthly sonde profiles for each region. The standard deviation between the individual launches is displayed in the plots. For some regions (e.g. Southern midlatitudes) only few stations and measurements are available and especially towards the end of the validation period the observations get sparse and the results are thus less representative.

3 Surface observations

3.1 GAW ozone and carbon monoxide

The Global Atmosphere Watch (GAW) programme of the World Meteorological Organisation (WMO) has been established to provide reliable long-term observations of the chemical composition and physical properties of the atmosphere, which are relevant for understanding long-term atmospheric chemistry trends and climate change (WMO, 2013). Within GAW, the focus is set on observations that are regionally representative and should be free from influence of significant local pollution sources and thus suited for the validation of global chemistry climate models (WMO, 2007).

The recommended routine measurement technique for O3 is UV absorption (see GAW report No 209, WMO 2013) and for CO, the analytical measurement techniques are NDIR, GC/HgO, GC/FID, VURF or QCL, (see GAW report No 192, 2010). For NRT data, no intensive data quality control has to be performed by the providers except the standard checks of the measuring equipment according to the Standard Operating Procedures (SOPs) or Measurements Guidelines (MGs) for the respective gases. For NRT O3 and CO GAW data, an uncertainty of 15% is acceptable: for surface ozone ±5ppb and for CO ±10ppb.

The current Near-Real-Time (NRT) validation relies on 12 GAW stations delivering O3 and 11 stations delivering CO surface mixing ratios (Fig. 3.1). Five stations (Hohenpeissenberg, Jungfraujoch, Sonnblick, Zugspitze and Monte Cimone are located in Europe. All of them are mountain stations.

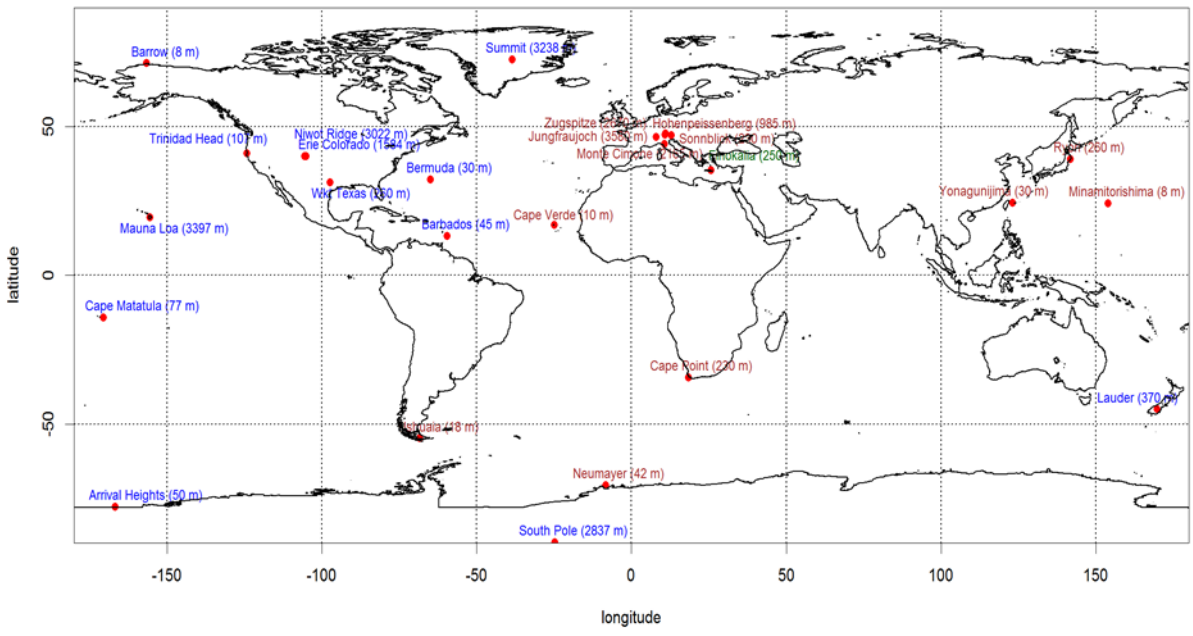

Figure 3.1: Map of the GAW (brown), ESRL (blue) and EMEP (green) validation stations.

Table 3.1. List of GAW and ozone sonde stations used for the validation.

Station/location	lat [°]	lon [°]	Altitude [m]	Instruments/species measured	type/network
Cape Point	-34.35	18.48	230	O3, CO surface	GAW
Cape Verde	16.85	-24.87	10	O3, CO surface	GAW
Hohenpeissenberg	47.8	11.02	985	O3, CO surface	GAW
Jungfraujoch	46.55	7.99	3580	O3, CO surface	GAW
Minamitorishima	24.29	153.98	8	O3, CO surface	GAW
Monte Cimone	44.18	10.7	2165	O3, CO surface	GAW
Neumayer	-70.65	-8.25	42	O3	GAW
Ryori	39.03	141.82	260	O3, CO surface	GAW
Sonnblick	47.05	12.96	3105	O3, CO surface	GAW
Ushuaia	-54.85	-68.32	18	O3, CO surface	GAW
Yonagunijima	24.47	123.02	30	O3, CO surface	GAW
Zugspitze	47.4	10.9	2670	O3, CO surface	GAW
Alert	82.4	-62.3	66	O3, free troposphere	sonde/NILU
Debilt	5.18	52.1	2	O3, free troposphere	sonde/NILU
Edmonton	53.5	-114	766	O3, free troposphere	sonde/NILU
Eureka	80	-86.5	10	O3, free troposphere	sonde/NILU
Goose Bay	53.2	-60.5	36	O3, free troposphere	sonde/NILU
Hohenpeissenberg	47.8	11	976	O3, free troposphere	sonde/NILU
Joikoinen	60.81	23.5	103	O3, free troposphere	sonde/NILU
Legionow	52.4	20.9	96	O3, free troposphere	sonde/NILU
Lerwick	60.14	-1.19	82	O3, free troposphere	sonde/NILU
Ny Alesund	79	12	17	O3, free troposphere	sonde/NILU
Prag	50	14.4	304	O3, free troposphere	sonde/NILU
Resolute	74.72	-94.98	200	O3, free troposphere	sonde/NILU
Scoresbysund	70.5	-22	76	O3, free troposphere	sonde/NILU
Sodankyla	67	27	179	O3, free troposphere	sonde/NILU
Uccle	51	4	100	O3, free troposphere	sonde/NILU
Hilo	19.4	-155	11	O3, free troposphere	sonde/SHADOZ
Java (Watukosek)	-8	113	50	O3, free troposphere	sonde/SHADOZ
Nairobi	-1	37	1795	O3, free troposphere	sonde/SHADOZ
Natal	-5.49	-35.26	14	O3, free troposphere	sonde/SHADOZ
Reunion	-21.06	55.48	24	O3, free troposphere	sonde/SHADOZ
Samoa (Cape Matatula)	-14	-171	77	O3, free troposphere	sonde/SHADOZ
Macquarie Island	-54.5	158.9	7	O3, free troposphere	sonde/WOUDC
Madrid	40.5	-3.8	631	O3, free troposphere	sonde/WOUDC
Marambio	-64.23	-56.62	198	O3, free troposphere	sonde/WOUDC
Naha	26.2	127.7	28	O3, free troposphere	sonde/WOUDC
Sapporo	43	141	26	O3, free troposphere	sonde/WOUDC
Tsukuba	36.06	140.13	31	O3, free troposphere	sonde/WOUDC
Ushuaia	-54.85	-63.32	17	O3, free troposphere	sonde/WOUDC
Valentia	51.9	-10.3	14	O3, free troposphere	sonde/WOUDC

Three stations (Ryori, Minamitorishima and Yonaguijima) are located in Japan: Ryori is situated on the pacific coast; the other two stations are island stations. Cape Verde is a coastal station. There are two stations located in the Southern Hemisphere: Ushuaia, placed on a remote sub-Antarctic marine coast and Neumayer in Antarctica. The three Japanese stations are classified as regional stations, all others are global stations. A detailed description of the stations and the specific requirements for classification are given at: http://gaw.empa.ch/gawsis/default.asp and http://gaw.empa.ch/gawsis/requirements.html.

For the validation, 6-hourly values (0:00, 6:00, 12:00, 18:00 UTC) of the analysis mode are extracted from the model and are matched with hourly observational GAW station data. Model mixing ratios at the stations' locations are linearly interpolated from the model data in the horizontal. In the vertical, modelled gas mixing ratios are extracted at the model level, which is closest to the GAW stations' altitude. Validation scores (MNMB, r) are calculated for each station on a quarterly basis (DJF, MAM, JJA, SON). Time series plots show the model runs in comparison with the observations.

3.2 ESRL Global Monitoring Division and EMEP surface ozone observations

Simulated Near-Real-Time (NRT) ozone mixing ratios were validated against observations provided by the ESRL Global Monitoring Division (http://www.esrl.noaa.gov/gmd/; Oltmans et al.,1994; McClure-Begley et al.,2014). The vast majority of measurements using for the validation were made using ozone monitors that use the absorption of ultraviolet (UV) radiation at 254 nm as the principle of measurement (see GAW report No 209, WMO 2013). Most of the measurements are tied to a network standard maintained by CMDL which is in turn linked by intercomparison with the standard ozone photometer maintained by the U.S. National Institute of Standards and Technology (For more information regarding instrument specifications and limits: http://www.thermoscientific.com/content/tfs/en/product/model-49-i-i-i-ozone-analyzer.html)

Thirteen ground-based stations, namely 1. Arrival Heights, Antarctica, New Zealand (ARH), 2. Tudor Hill, Bermuda, United Kingdom (BER), 3. Barrow, Alaska, United States (BRW), 4. Eureka, Canada (EUK), 5. Lauder, New Zealand (LDR), 6. Mauna Loa, Hawaii, United States (MLO), 7. Niwot Ridge, Colorado, United States (NWR), 8. Ragged Point, Barbados (BAR), 9. South Pole, Antarctica (SPO) 10. Summit, Greenland, (SUM), 11. Table Mountain, Colorado, United States (TBL), 12. Trinidad Head, California, United States (THD) and 13. Tiksi, Russia (TIK) were included in the validation scheme. In the validation process additional data from one EMEP station in the Mediterranean, namely 14. Finokalia (FK) are used. The majority of these sites are generally free from local sources of contamination. At two of the sites-Barrow and Bermuda, the locally contaminated measurements can be screened using the local wind direction. Note that at Mauna Loa, the strong mountain wind circulation separates the measurements in to upslope and downslope conditions. During the daytime, upslope regime boundary layer air is mixed with the free tropospheric air, while during nighttime downslope flow, free tropospheric air is sampled (Oltmans and Komhyr, 1986).

The uncertainty required for NRT surface data delivery is less than ± 5 nmol/mol for hourly values of unvalidated data. Detailed information on the ESRL O_3 measurements can be found in Oltmans et al, 1994.

Data QA/QC: The quality of data is a joint effort by the program managers and the station technicians.

Table 3.2: Coordinates of stations and number of Obs (3-hourly) used in the present validation analysis.

Station	Latitude	Longitude	Altitude (m)	Country	Number of Obs during period 01/09/2015 - 30/11/2015
Station	**Latitude**	**Longitude**	**Altitude (m)**	**Country**	**Latitudinal Zone**
Eureka (EUK)	80.05°N	86.42°W	610	Canada	Arctic
Summit (SUM)	72.57°N	38.38°W	3266	Greenland	Arctic
Tiksi (TIK)	71.58°N	128.92°E	8	Siberia, Russia	Arctic
Barrow (BRW)	71.32°N	156.61°W	8	Alaska, United States	Arctic
Trinidad Head (THD)	41.05°N	124.15°W	107	California, United States	USA; NH mid-latitudes
Table Mountain (TBL)	40.12°N	105.24°W	1689	Colorado United States	USA; NH mid-latitudes
Niwot Ridge (NWR)	40.04°N	105.54°W	3022	Colorado United States	USA; NH mid-latitudes
Finokalia (FK)	35.32°N	25.67°E	250	Greece	Mediterranean; NH mid-latitudes
Bermuda (BER)	32.27°N	64.88°W	30	United Kingdom	Tropics
Mauna Loa (MLO)	19.54°N	155.58°W	3397	Hawaii, United States	Tropics
Ragged Point (BAR)	13.17°N	59.46°W	45	Barbados	Tropics
Lauder (LDR)	45.04°S	169.68°E	370	New Zealand	SH mid-latitudes
Arrival Heights (ARH)	77.80°S	166.78°W	50	New Zealand, Antarctica	Antarctica
South Pole (SPO)	90.00°S	24.80°W	2837	Antarctica	Antarctica

For the validation, 3-hourly model values have been interpolated linearly in the horizontal at the stations' location (see Table 3.1, 3.2 and Fig. 3.1). In the vertical, simulated ozone concentrations have been extracted at the model level that matches the real altitude of the stations, which is equivalent to matching the mean pressure of model level and station. Validation scores (MNMB, r) are calculated for each station on a quarterly basis (DJF, MAM, JJA, SON). Time series plots show the model runs in comparison with the observations.

4 IASOA surface observations in the Arctic

Simulated Near-Real-Time (NRT) ozone mixing ratios are validated against observations provided by the IASOA network (http://www.esrl.noaa.gov/psd/iasoa/).

4.1 Villum Research Station, Station Nord, Greenland

Half-hour values of Ozone are measured with an UV absorption monitor, API, with a detection limit of 1 ppbv and an uncertainty of 3% for concentrations above 10 ppbv and 6% for concentrations below 10 ppbv (all uncertainties are at a 95% confidence interval). From December 2015 two monitors are measuring in parallel.

Ozone measurements in Denmark are performed under EN 17025 accreditation. It is not possible to follow the standards at the Villum Research Station due to the long distance from civilization and difficult logistics. However, the measurements are made as close as possible to the accreditation and the fewer visits possible is compensated by using 2 instruments for ozone monitoring (Skov et al. 2004, Heidam et al. 2004 and Skov et al. 2016; under preparation). The data are validated within a six months period after the data acquisition. The measurement site is located 2 km away from the military station, Station Nord, and thus local influence on ozone concentrations is at a minimum.

Measurements are aggregated to 3-hour averages to match the temporal resolution of the model. Model values have been interpolated linearly in the horizontal at the location of the stations. In the vertical, simulated ozone concentrations have been extracted at the model level that matches the real altitude of the stations. The average value is used for model validation when both monitors are operational. Error bars and uncertainties on the measurements are not applied in the analyses.

Table 4.1: Coordinates of stations and list of species used in the present validation analysis.

Station	Latitude	Longitude	Altitude (m)	Country	Species
Villum Research station, Station Nord (VRS)	81o 36'5.26" N	39'43.31" W	24	Greenland	O_3

5 Airbase surface observations in the Mediterranean

For ground-level concentrations, we use observations from the European Air quality database (AirBase; http://acm.eionet.europa.eu/databases/airbase/) which is the public air quality database system of the European Environmental Agency (EEA; http://www.eea.europa.eu/). AirBase contains air quality monitoring data and information from the European Environment Information and Observation Network (EIONET) submitted by the participating countries throughout Europe. The air quality database consists of multi-annual time series of air quality measurement data and their statistics for a representative selection of stations and for a number of pollutants. It also contains meta-information on the involved monitoring networks, their stations and their measurements.

For the aerosol NRT evaluation, the data catalogue included the LIVE Air Quality Data service (http://discomap.eea.europa.eu/map/fme/AirQualityUTDExport.htm), which is the up-to-date (UTD) air quality data provided by EEA, is used, including PM10 and PM2.5 data. The download service provides access to UTD air quality data reported to EEA on hourly basis from EEA member countries. Depending on the member country a delay of some hours is expected from the measurement is taken until it is available in the download service. The delay is normally between 1 and 6 hours but it can take longer depending on the infrastructure setup in the specific country. The UTD dataflow is voluntary and the list currently counts 20 countries, additional countries are expected to join in 2016. To see the current status on data delivery (Fig. 5.1), which

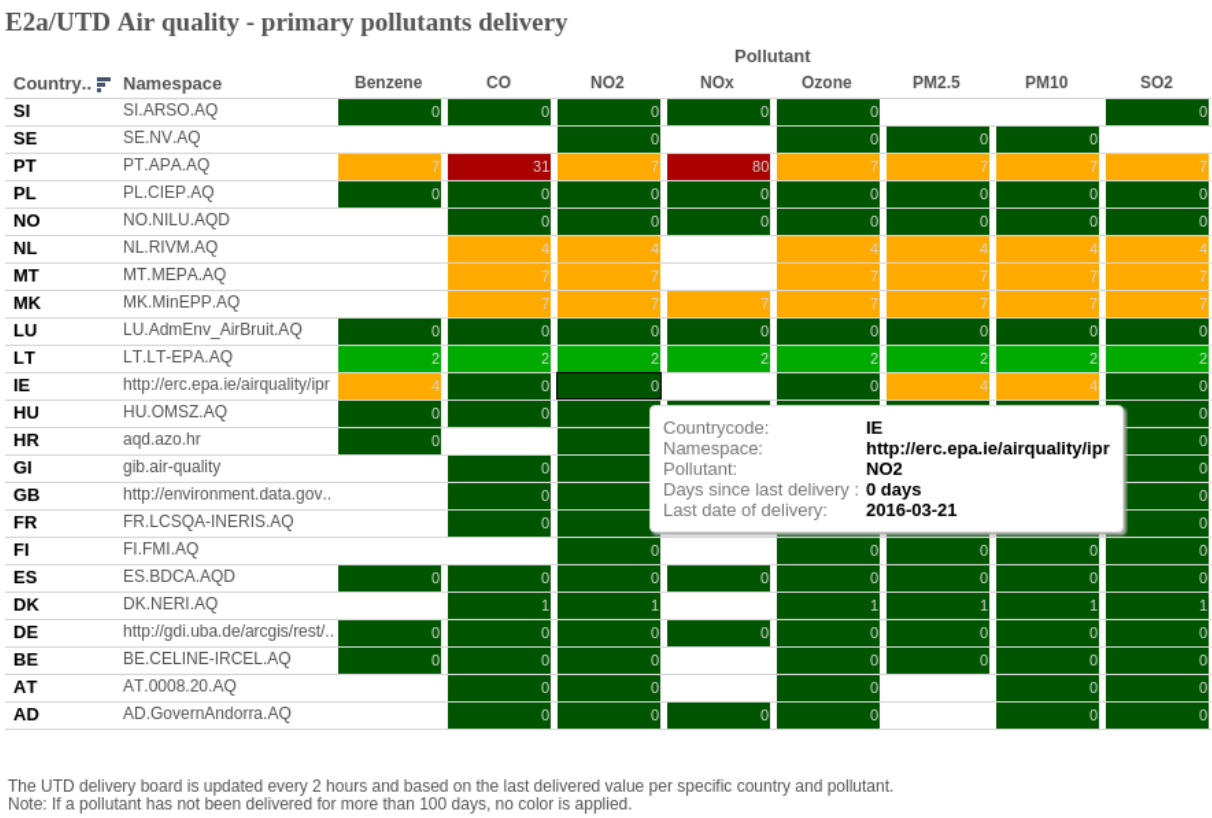

Figure 5.1. Snapshot of the UTD report on data delivery for 21 March 2016.

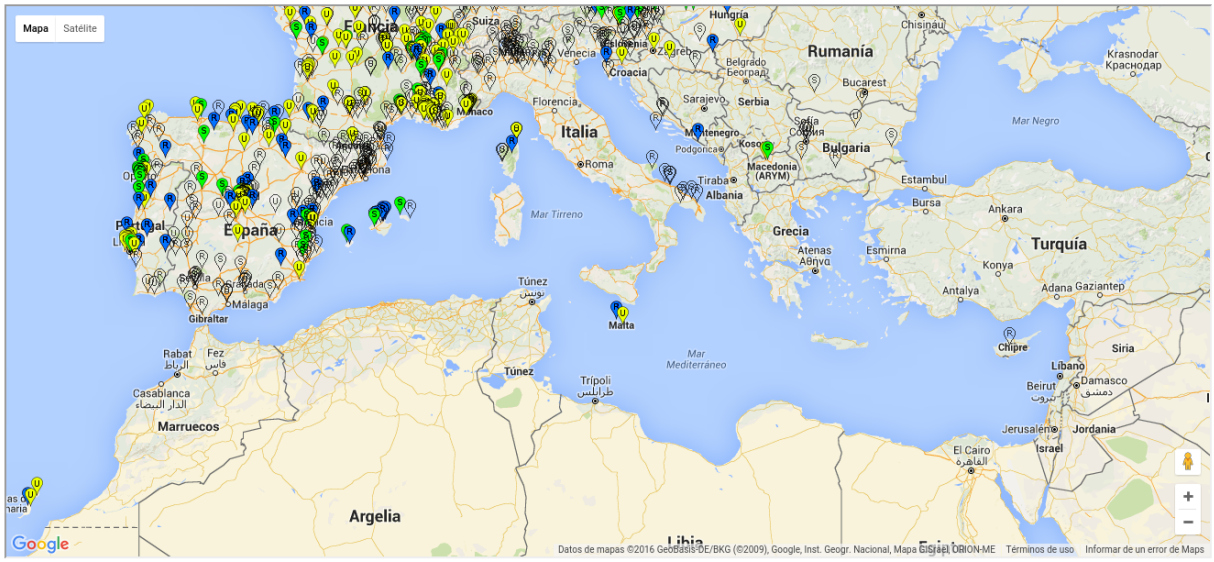

Figure 5.2. Available NRT PM10 Airbase background sites in Airbase for March 2016 in colours: urban is yellow, green is suburban and blue is rural.

countries are delivering data and what they deliver. See the following report: https://tableau.discomap.eea.europa.eu/#/site/Aironline/views/Airquality_E2a_monitoring/DashboardE2a?:iid=10

The data offered via this service is provided as delivered by the member countries to EEA. EEA are not responsible for the quality or the correctness of the data.

Only those stations considered as background (rural, suburban and urban) sites in the Airbase catalogue are considered in the aerosol validation. All NRT PM10 and PM2.5 available measurements (i.e. no-validated observations) within ±60 min of the models' outputs are used for the 3-hourly evaluation. CAMS model outputs (PM10 and PM2.5) are bilinear interpolated in the horizontal at the stations' location (see Figure 5.2).

Three-hourly values of PM10 and PM2.5 from AirBase and CAMS model outputs are used to check the model performance. Mean Bias (MB), Fractional Gross Error (FGE), Root Mean Square Error (RMSE), Person correlation coefficient (r), and the number of data (NDATA), averaged over the study period are computed for this objective. This set of statistics is being computed for each site over the Mediterranean (shown in Figure 5.2).

Simulated Near-Real-Time (NRT) ozone mixing ratios are validated against observations provided by Airbase (http://acm.eionet.europa.eu/databases/airbase/). The data are downloaded through an FTP created by Meteo France (ftp.cnrm-game-meteo.fr/TEST/). All available stations with surface ozone observations for period September-November 2015 are shown in figure 5.3.

The model performance has been carried out using all available stations in the Mediterranean that fulfil the criteria shown in Table 5.2. Table 5.1 shows names and coordinates for each one of the selected Mediterranean stations.

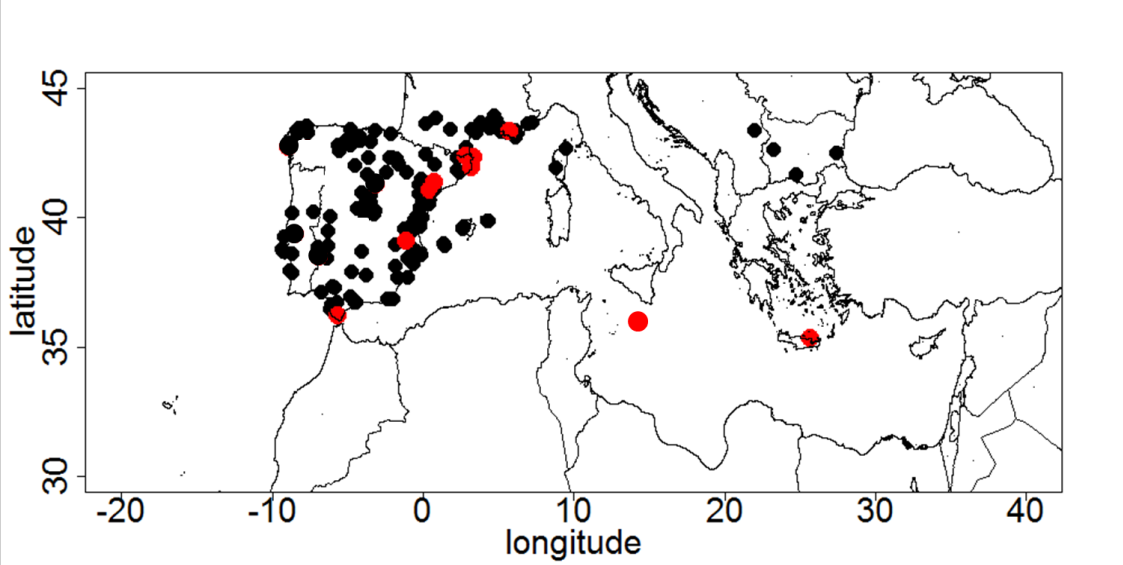

Figure 5.3. Available NRT surface ozone Airbase sites for period September-November 2015. With red cycles are denoted stations that fulfil the criteria shown in Table 2.

Model values have been interpolated linearly in the horizontal at the stations' location (see Table 5.1). In the vertical, simulated ozone concentrations have been extracted at the model level which matches the real altitude of the stations, which is equivalent to matching the mean pressure of model level and station. Validation scores (DJF, MAM, MNMB, r) are calculated for each station on a quarterly basis (SON). Time series plots show the model runs in comparison with the observations.

Table 5.1: Coordinates, elevation as, for each one of the selected Mediterranean stations.

Station Name	Stat_ID	Lon	Lat	Elevation (m)	Distance from the shore (km)
Al Cornocales	ES1648A	-5.66	36.23	189	16
Caravaka	ES1882A	-1.87	38.12	1	73
Zarra	ES0012R	-1.10	39.08	885	70
VIillar Del Arzobispo	ES1671A	-0.83	39.71	430	48
Cirat	ES1689A	-0.47	40.05	466	37
Bujaraloz	ES1400A	-0.15	41.51	327	60
Morella	ES1441A	-0.09	40.64	1150	51
Bc-La Senia	ES1754A	0.29	40.64	428	21
Ay-Gandesa	ES1379A	0.44	41.06	368	15
Ak-Pardines	ES1310A	2.21	42.31	1226	81
Hospital Joan March	ES1827A	2.69	39.68	172	3
Al-Agullana	ES1201A	2.84	42.39	214	25
Av-Begur	ES1311A	3.21	41.96	200	9
Plan Aups/Ste Baume	FR03027	5.73	43.34	675	21
Gharb	MT00007	14.20	36.07	114	31
Aliartos	GR0001R	23.11	38.37	110	18
Finokalia	GR0002R	25.67	35.32	250	4

Table 5.2: Criteria for the selection of stations.

1)	Station was selected from classes 1-2 in the O3 Joly-Peuch classification
2)	Station was identified as 1-2 in NO2 and NO Joly-Peuch classification when NOx data were available
3)	Data availability at each station to exceed 80% of all possible points during 2005-2012
4)	Statistically significant correlations between observed air temperature at 850hPa and surface ozone
5)	Station located within about 100 km from the shoreline of the Mediterranean

6 IAGOS aircraft measurements

The IAGOS program (Petzold et al, 2015) uses sensors mounted on commercial aircraft to obtain in situ measurements of various chemical species in the atmosphere. All IAGOS-CORE aircraft are equipped with a package which provides volume mixing ratios of the trace gases O3, CO, and water vapour, cloud particle number concentration, and meteorological measurements including temperature, pressure and winds. Further details of the O3 and CO instruments and their operation can be found in Nédélec et al. (2015). Data are stored every 4s throughout the flight, and are used either as tropospheric profiles taken during landing and take-off or as horizontal trajectories in the upper troposphere-lower stratosphere (UTLS) obtained during the cruise part of the flight. The IAGOS network is shown in figure 1. So far the IAGOS fleet has visited 156 airports. More details on the frequency of the airports visited by IAGOS are available on the IAGOS website at http://www.iagos.fr/web/rubrique11.html. The airports are spread over latitudes ranging from -37°S (Melbourne) to 64°N (Fairbanks). Most airports serve large urban conglomerations where pollution would be expected to be high. Most airports are also located in coastal areas and are obviously free of vegetation. Otherwise, the airports are representative of a wide variety of environments. Petetin et al (2017) addressed the representativeness of IAGOS measurements in the lower troposphere and have found that in the first few hundred metres above the surface, IAGOS profiles can be considered as suburban or urban background stations shifting towards regional representativness as altitude increases.

Data are transmitted when the aircraft arrives at its parking gate, and are available for use in CAMS after a time-delay of a few days (ideally less than 3). This time-delay is to enable the project PI to give a first check of the data. This is the first stage in the QA/QC procedure that is fully described in Nédélec et al. (2015). The measurement accuracy of ozone is estimated at ±[2 ppbv + 2%] and for CO ±[5 ppbv + 5%]. These values are independent of geographic location and altitude. Sometimes two aircraft arrive or depart from the same airport within 3 hours, which offers an opportunity to crosscheck the measurements from two different aircraft. Nearly 1000 intercomparisons have been made so far. Similarly, two aircraft may fly along a similar trajectory at cruise altitude enabling a crosscheck of the instruments in the UTLS. This happens less frequently (147 so far) but is still an important check on the performance of the instruments.

Additionally, each instrument's zero and calibration factor are regularly checked in-flight. For ozone, this calibration is performed every two hours. Similarly for CO, checks are made every 20 minutes or if the temperature of the instrument increases by more than 1K. The purpose of these checks is primarily to check for instrument drift. At the end of their operational period (approximately 6 months) the instruments are removed from the aircraft and calibrated in the laboratory. This calibration is performed with a reference analyser, which is periodically crosschecked with a primary standard at the National Institute of Standards and Technology in France. Due to the 6 month wait, these calibrated data are not available for use the in the NRT reports but are usually ready for evaluation with the reanalysis. From the beginning of the MOZAIC program in 1994 (Marenco et al., 1998), the measurement quality control procedures have remained unchanged ensuring that the time-series are free of instrumental artefacts, which is vital for the evaluation of the reanalysis.

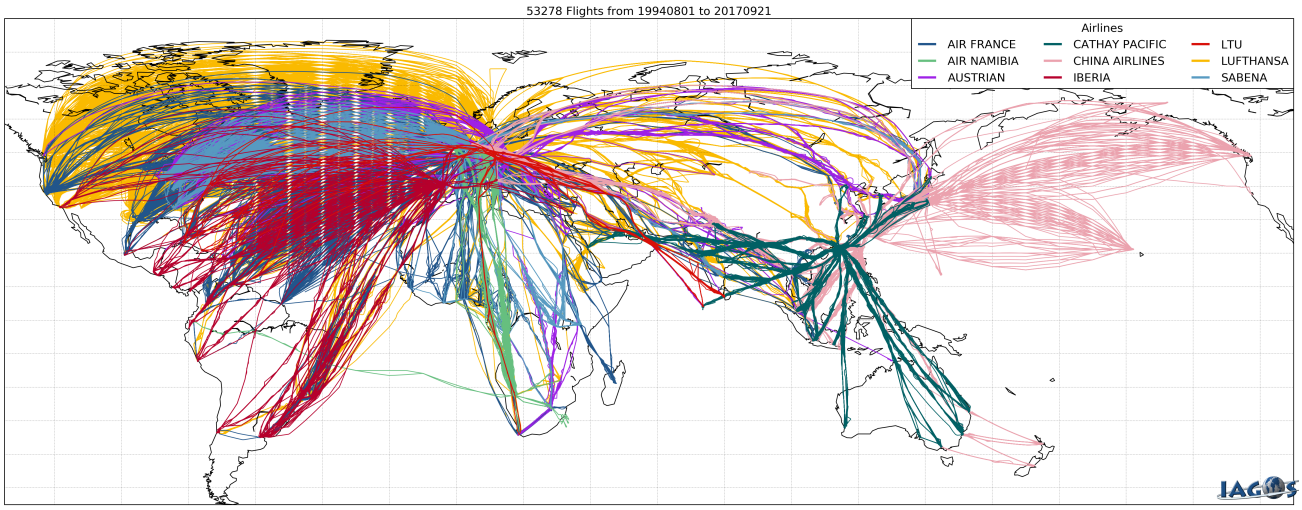

Figure 6.1. IAGOS flights since July 2011.

6.1 Validation Methodology

Global

Ozone and CO profiles from IAGOS-CORE (in NRT) obtained during landing and take-off are used in the reports with additional profiles from IAGOS-CARIBIC used for the evaluation of the reanalysis. Frankfurt has the most consistent availability of data dating back to the beginning of MOZAIC in 1994. Other airports are included in the report if they are considered to be of interest and if the availability of data is good. For example, there is a high frequency of flights to airports in the Gulf of Guinea (Lagos, Port Harcourt, Malabo) and West Africa (Luanda and Abuja) and frequent flights to the Arabian Peninsula (Muscat, Doha, Jeddah, Manama, Riyadh, Kuwait). Eastern North America (New York, Chicago, Philadelphia) and Asia (Taipei, Hong Kong) are also included.

A mean profile is calculated from the observations, which is the average of all the take-offs and landings at that airport for that day. This is compared with the profile extracted from the model's grid-box containing the airport. A daily mean is calculated from the forecast times. We present these daily mean profiles, and seasonal time-series of the daily mean mixing ratios calculated for 5 different atmospheric layers. The layers are: the surface layer extending up to 950hPa, the boundary layer from 950-850 hPa and the free troposphere from 850hPa to the upper troposphere. The height of the tropopause (if encountered) is determined from the IAGOS temperature profiles and the upper troposphere (UT) is defined as being 1km below the tropopause and the lower stratosphere (LS) 1km above the tropopause.

Regional

Ozone and CO profiles from IAGOS-CORE (in NRT) obtained during landing and take-off at European airports are used. Observations in ppbv are converted to µg/m3 using the IAGOS temperatures and pressures. Frankfurt and Paris have up to four flights per day. Other airports such as Vienna and Amsterdam are visited more infrequently. Unlike for the validation of the global models, the profiles are not averaged over a day. The models are interpolated to the flight track using the closest hour to the time of the profile, and from the 24-, 48-, and 72-hour preceding forecasts.

7 MOPITT and IASI CO observations

The IASI is nadir looking thermal infrared (TIR) sounder instruments on-board the satellite MetOp-A. It is designed to measure the spectrum emitted by the Earth-atmosphere system in the TIR spectral range, using nadir geometry. The IASI has been launched in October 2006 (Clerbaux et al., 2009) and provides global Earth coverage twice a day, with a horizontal resolution of 12 km diameter footprint on the ground at nadir. We use MetOp-A CO total column data, version v20100815 from 1st October 2007 to 29 September 2014 and version v20140922 from 30 September 2014. These data have been processed at LATMOS using a retrieval code, FORLI (Fast Optimal Retrievals on Layers for IASI), developed at ULB (Université Libre de Bruxelles). The IASI CO product is available at http://www.pole-ether.fr. Following the recommendations of Hurtmans et. al., 2012 we filter the data with bias values lower/higher than -0.15/0.25 x 10^{-9} W/(cm^2 cm^{-1} sr) and RMS larger than 2.7 x 10^{-9} W/(cm^2 cm^{-1} sr). Also we filter the data with CO total column > 20 x 10^{18} molec/cm^2. And only the data with "super" quality flag is equal to 0 were used. The estimated accuracy of the CO data is < 10% (George et al., 2009).

The MOPITT instrument is mounted on-board the NASA EOS Terra satellite and has been operational since March 2000 (Deeter et al., 2010). It measures upwelling radiation in the thermal infrared spectral range using gas-filter correlation radiometry. At nadir view, the MOPITT instrument has a horizontal resolution of 22 x 22 km^2 and allows for global coverage within three days. The data used corresponds to the daytime CO total columns from the versions 5 (V5) and 6 (V6) of the MOPITT thermal infrared product level 3. As the processing and deliveries of the MOPITT V5 products concluded at the end of 2016, from then on, MOPITT V6 is used for the validation. This product is available via the following web server: http://www2.acd.ucar.edu/mopitt/products. Validation of the MOPITT V5 product against in situ CO observations shows a mean bias of 0.06 x 10^{18} molecules cm^{-2} (Deeter et al., 2013). The MOPITT V6 product incorporated the following features: improved geolocation data, the new CO climatology based on CAM-cem simulations for 2000-2009, meteorological profiles which are interpolated from the NASA MERRA reanalysis product (instead of NCEP for V5). The bias of MOPITT V6 total column data has been reduced to 0.03 x 10^{18} molecules cm^{-2} (Deeter et al., 2014). Following the recommendation in the user's guide (www.acd.ucar.edu/mopitt/v5_users_guide_beta.pdf), the MOPITT data are averaged by taking into account their relative errors provided by the observation quality index.

For the validation, the modeled CO profiles are first averaged monthly for each forecastday (d0, d2, d4) (units: CO(time, level, latitude, longitude) [kg/kg]). Then the monthly mean CO profiles are transformde from CO[kg/kg] to volume mixing ratio:

VMR CO [mole/mole] = CO[kg/kg] /(28.01/28.96) and regridded to the same grid as used for the MOPITT gridded data (1x1TM5), with conserved mass. The monhtly averaged modeled CO profiles (X) are transformed by applying the satellite averaging kernels (A) and the a priori CO profile (X_a) according to the following equation (Rodgers, 2000) to create the profiles X^* appropriate for comparison with satellite data:

$$\boldsymbol{X^* = X_a + A(X - X_A)}$$

The averaging kernels indicate the sensitivity of the satellite measurement and retrieval system to the true CO profile, with the remainder of the information set by the a priori profile and retrieval constraints (Emmons, 2009; Deeter et al., 2010). The model CO total columns, used in the comparison with satellite observations, have been calculated using the profiles $\boldsymbol{X}^*$ which have the same vertical resolution and a-priori dependence as the satellite retrievals.

The averaging kernels indicate low sensitivity near the surface and maximum sensitivity in the low troposphere (4–6 km), where MOPITT shows slightly higher sensitivity compared to IASI (George et al., 2009).

8 SCIAMACHY/GOME-2 observations

The Scanning Imaging Spectrometer for Atmospheric Chartography (SCIAMACHY, Bovensmann et al., 1999) is an UV/visible/near infrared spectrometer, which operated on Envisat from August 2002 to March 2012 when the European Space Agency lost contact to the satellite. SCIAMACHY observed the light scattered in the atmosphere in nadir and limb geometry and also performed solar and lunar occultation measurements. Tropospheric trace gas columns can be derived from the nadir measurements at spatial resolutions of 30 x 60 km^2 for most gases with global coverage achieved after 6 days of observations. Envisat was in a sun-synchronous orbit with a descending node equator crossing time of 10:00 LT. SCIAMACHY raw radiances and irradiances are calibrated and distributed by DLR, the level 1 data version used by the IUP, University of Bremen in house DOAS retrievals used for analysis of trace columns in this project correspond to V7.04. The DOAS analysis applied to the SCIAMACHY data is described by Richter et al. (2005) for NO_2 and by Wittrock et al. (2006) for HCHO.

The Global Ozone Monitoring Experiment-2 (GOME-2) is a nadir viewing UV/visible spectrometer observing scattered sunlight in the spectral range from 240 to 790 nm with moderate spectral resolution of 0.26 to 0.51 nm (Munro et al., 2016). The first GOME-2 operating on MetOp-A provides data since January 2007, the second instrument on MetOp-B since December 2012. Both satellites are in sun-synchronous morning orbits with descending node equatorial crossing times of 09:30 LT. The spatial resolution of the instruments is 40 x 80 km^2 in nominal operation, providing nearly global coverage every day. For GOME-2 on MetOp-A this was changed to 40 x 40 km^2 in July 2013, improving spatial resolution at the expense of coverage.

Raw radiances and irradiances measured by the GOME-2 instruments are calibrated by EUMETSAT and the resulting level 1 data distributed in near real time (NRT) via EUMETCAST. Data is received at the IUP, University of Bremen and analysed for trace gas columns using in-house DOAS retrievals (Richter et al., 2011; Vrekoussis et al, 2010). The data sets used for CAMS validation are based on the NRT level 1 data and are not updated by the consolidated data, which is available at EUMETSAT after a few days or reprocessed data, which is provided by EUMETSAT at irregular intervals. The level 1 data version is therefore not consistent through the data set, meaning that different level 1 data versions are used for model validation. Data reception through EUMETCAST is sometimes interrupted for technical reasons or due to poor weather conditions leading to loss of connection. Most missing data is added within a few days, but some gaps remain in the IUP data set.

As the European Space Agency lost contact to Envisat in April 2012, SCIAMACHY data is used for validation prior to that date and GOME-2/MetOp-A data is used for all subsequent, recent comparisons.

8.1 Tropospheric NO_2

Tropospheric NO_2 columns are computed from level 1 SCIAMACHY/GOME-2 data using a three-step approach:

1) Applying the DOAS retrieval to measured spectra which yields the total slant column,

2) Correction of the stratospheric contribution by applying the reference sector correction approach,

3) Conversion into vertical columns by application of an air mass factor.

In addition, a chi-square limit of 5 x 10^{-3} is applied to the results of the DOAS fit and only observations with solar zenith angles between 0 and 85° are regarded. Only data with a FRESCO+ (Wang et al., 2008) cloud fraction smaller than 0.2 are used but no further cloud correction is applied.

Monthly mean tropospheric NO_2 columns are associated with relative uncertainties of roughly 20% - 30% in polluted regions with an additional absolute uncertainty of 5 x 10^{14} molec/cm^2. These are broad error estimates only. Therefore, in future NRT reports, standard deviations derived from monthly mean values for each specific month will be added to the satellite time series of tropospheric NO_2 columns as a first estimate on how the model simulated values compare to satellite retrievals.

The data product used here has some limitations mostly due to the simplistic stratospheric correction, which can lead to negative NO_2 columns at high latitudes in spring. The air mass factors are based on a monthly climatology created from one year of MOZART model profiles and thus cannot reproduce short-term variations in meteorology or biomass burning activity. However, for the purpose of verification, the most important point is to have a product that is completely independent from the models and data sources used in the CAMS system. This is the case for the product provided here.

8.2 Stratospheric NO_2

It is important to note that the SCIAMACHY/GOME-2 stratospheric columns are in fact total columns derived using a stratospheric air mass factor. To minimize the impact of the troposphere, only data over the clean Pacific region are used (180°E - 220°E). Still, the amount considered here as being stratospheric includes a weighted part of tropospheric NO_2.

A chi-square limit of 5 x 10^{-3} is applied to the results of the DOAS fit and only observations with solar zenith angles between 0 and 85° are regarded. No cloud screening is applied.

Monthly mean stratospheric NO_2 columns are associated with relative uncertainties of roughly 5 % - 10% and an additional absolute uncertainty of 1 x 10^{14} molec/cm^2 (these values are only valid over the clean Pacific). These are broad error estimates only. Therefore, in future NRT reports, standard deviations derived from monthly mean values for each specific month will be added to the satellite time series of stratospheric NO_2 columns as a first estimate on how the model simulated values compare to satellite retrievals.

8.3 Tropospheric HCHO

Tropospheric HCHO columns are computed under the assumption that stratospheric HCHO amounts are negligible. HCHO columns are derived from level 1 SCIAMACHY/GOME-2 data using the DOAS

method. Air mass factors are based on a static monthly climatology using land surface classification and biomass burning statistics to estimate the vertical HCHO profile.

A chi-square limit of 2 x 10^{-3} is applied to the results of the DOAS fit from GOME-2 data and only observations with solar zenith angles between 0 and 60° are used. For SCIAMACHY the solar zenith angle limits are the same, but the chi-square limit is 2.5 x 10^{-4}. For GOME-2, only data with a FRESCO+ cloud fraction lower than 0.2 are used but no further cloud correction is applied. As the SCIAMACHY/GOME-2 HCHO retrievals are subject to drifts and offsets, the values are normalized over the Pacific sector.

Monthly mean HCHO columns are associated with relative uncertainties of roughly 10% - 30% and an additional absolute uncertainty of 2 x 10^{15} molec/cm^2. As these uncertainty estimates are much larger than for NO_2, data are smoothed to reduce the impact of noise. The error estimates are broad values only. Therefore, in future NRT reports, standard deviations derived from monthly mean values for each specific month will be added to the satellite time series of tropospheric HCHO columns as a first estimate on how the model simulated values compare to satellite retrievals. HCHO column data in the region of the South Atlantic Anomaly are not valid and are therefore not regarded for model validation.

8.4 Treatment of model data

The first step consists in selecting the model output corresponding to the satellite overpass time (approx. 10:00 solar local time (LT) for SCIAMACHY, 09:30 LT for GOME-2).

The model results are then integrated in the vertical to derive tropospheric and stratospheric vertical columns, as only vertical columns are retrieved from the satellite measurements and not concentrations at specific heights. For the separation of the stratosphere and troposphere, a latitude dependent tropopause height is used.

The spatial resolutions of the models are coarser than that of the standard SCIAMACHY/GOME-2 product (0.125° x 0.125°). Thus, the daily satellite measurements are re-gridded to the corresponding model resolution of 0.4° for C-IFS runs. In this process, the average of all valid SCIAMACHY/GOME-2 grid boxes within one model grid box is taken without applying any area weighting, i.e., all satellite data are considered as long as part of it is located within the model box.

Finally, the model data is selected according to the existing satellite data, ensuring that both datasets consist of data for the same days at the same locations. This is important because for example SCIAMACHY data are not available at daily global coverage. In optimal conditions, the global coverage would be obtained every 6 days. Moreover, with the exception of SCIAMACHY HCHO, tropospheric columns are only determined for clear sky pixels, i.e., cloud fraction smaller than 20% according to the FRESCO+ data. For this reason, the daily model data previously selected for the overpass time are then matched to the available SCIAMACHY/GOME-2 data, which is already converted to the model resolution.

In order to get sufficient signal to noise ratio and statistical representativeness, all data are considered as monthly averages only.

9 Aerosol and dust optical depth from AERONET

High quality aerosol optical properties are provided by the ground-based sun-/sky photometer networks of AERONET (Aerosol, Robotic NETwork; Holben, 2001: http://aeronet.gsfc.nasa.gov/) programme. The AERONET program provides a long-term, continuous and readily accessible public domain database of aerosol optical, microphysical and radiative properties for aerosol research and characterization, validation of satellite retrievals, validation of aerosol models, and synergism with other databases. The network imposes standardization of instruments, calibration, processing and distribution.

Holben et al. (1998) and Eck et al. (1999) found relative uncertainties for reference AERONET instruments better than 0.2–0.5 and 1.5% for field instruments in the visible and the near-infrared range (Ecket al., 1999; Schmid et al., 1999). This means an uncertainty due to calibration between 0.002 and 0.005 for reference instruments and 0.015 for instruments calibrated by means of intercomparison techniques and regular inter-annual checks in calibration laboratories.

Since October 2015, AERONET recommends the new CE318-T (Triple) instrument (see AERONET news at http://aeronet.gsfc.nasa.gov/), which has been designed to perform a complete cycle of diurnal photometric measurements during both daytime and night-time (Barreto et al., 2016). The CE318-T, with new improvements that permit to extend photometric information at night-time using the moon as a light source, will replace the standard AERONET Cimel sunphotometer.

In their comprehensive assessment evaluation of the new CE318-T, following the error propagation theory, Barreto et al. (2016) provided an estimation of the combined CE318-T AOD standard uncertainty for each calibration method. For the daylight period Barreto et al. (2016) expect similar values to those calculated for standard sunphotometer versions, ranging between 0.002 and 0.009 for reference instruments and 0.015 for field instruments. For the night-time period, Barreto et al. (2016) estimate AOD uncertainty values of 0.011–0.014 for visible channels (with the exception of 440 nm, with values up to 0.016 for higher phase angles) and 0.012–0.018 for near-IR channels. For field instruments calibrated using the Moon Ratio technique they found AOD uncertainty between 0.011 and 0.019. Using the new Sun Ratio technique (Barreto et al., 2016), higher uncertainties are expected: 0.012–0.015 (0.017) for visible (440 nm) channels and 0.015–0.021 for longer wavelengths. For instruments calibrated by means of the new Sun-Moon gain factor technique (Barreto et al., 2016), the uncertainties range from 0.016 to 0.019.

AERONET provides globally distributed observations of spectral aerosol optical depth (AOD), inversion products, and precipitable water in diverse aerosol regimes. AERONET has been operating under what we call Version 2 processing that we implemented in 2006 and was based on 2004 knowledge and expertise. The newest processing, Version 3, was released in 2015 after the entire database was reprocessed and real-time data processing became operational (http://aeronet.gsfc.nasa.gov/cgi-bin/print_web_data_v3). All Version 3 algorithms have been developed individually vetted and represent four main categories: aerosol optical depth (AOD) processing, inversion processing, database management and new products. The primary trigger for release of Version 3 lies with cloud screening of the direct sun observations and computation of AOD that will fundamentally change all data available for analysis and all subsequent retrieval products. Aerosol optical depth data are computed for three data quality levels: Level 1.0

(unscreened), Level 1.5 (cloud-screened), and Level 2.0 (cloud-screened and quality-assured). The main difference between Level 1.5 and Level 2.0 datasets, is that Level 1.5 dataset is corrected with the pre-calibration (performed to the photometer before start measuring on a site), while Level 2.0 data are corrected with pre- and post-calibration. The latter is applied once the photometer has been post-calibrated after having been measuring for about a year in an AERONET station. In many cases the differences between Level 1.5 and Level 2.0 data is very small, less than the associated AOD uncertainty, however undetected cloud contamination may give bias to level 1.5 data.

Currently, the network is composed by more than 300 sunphotometers around the world (http://aeronet.gsfc.nasa.gov/Site_Lists/site_index.html). AERONET-Europe Central Facility provides instrument calibration and data processing of the new CE318-T photometers for the night period, within ACTRIS-2 project.

9.1 Method for comparison of AOD at global scale

Global model evaluation is performed regularly to document the CAMS aerosol performance. AeroCom type evaluation is generated every second week of a given month since April 2011. Version 3 Level 1.5 NRT Aeronet Data are obtained from the NASA Goddard webserver. Standard score tables, maps, scatterplots, bias maps, time series comparison and histograms are made available through the AeroCom web interface http://aerocom.met.no/cgi-bin/aerocom/surfobs_annualrs.pl?PROJECT=CAMS. The performance of the o-suite and e-suite can this way be compared to other model simulations, such as earlier MACC model versions, the MACC reanalysis or the AeroCom Median from an international multi-model ensemble.

The analysed variables consist of the total aerosol optical depth (AOD) at 550 nm and the Angstöm coefficient. Since sun photometers measure AOD at 500 nm, an Angström coefficient is obtained from 440nm and 670nm AOD values and is used to obtain from AOD@500nm an approximate AOD@550nm value. Mountain sites above 1000 m are excluded from comparison because model orography often does not reflect real orography. The 3-hourly model data are retrieved finally on the days when valid, clear-sky Aeronet observations in the model grid are reported. No observation is available on cloudy days and during night. Depending on region and season sampling frequency at a given station may vary largely from absent to daily observation through a full month. Coherent pairs of valid daily observation from model and sun photometer are retained at each station. To further filter out possibly cloud contaminated NRT data, daily Aeronet data are rejected when the measured Angström coefficient is less than 0.2 and if, on the same day, the observation is twice as large as the corresponding CAMS o-suite model value. The varying fluctuating network comprises ca 300 sites. A site location map of where stations with valid observations are located in June 2017 is found in figure 9.1.

Valid daily data from all stations over the globe are used to form the comparison basis for a given month. Standard score tables, maps, scatterplots, bias maps, time series comparison, histograms and site location maps are made available through the AeroCom web interface http://aerocom.met.no/cgi-bin/aerocom/surfobs_annualrs.pl?PROJECT=CAMS for each month. Site location maps and time series plots can be used to trace back which data went into statistical performance parameters for a given month. The performance of the o-suite and e-suite can in this

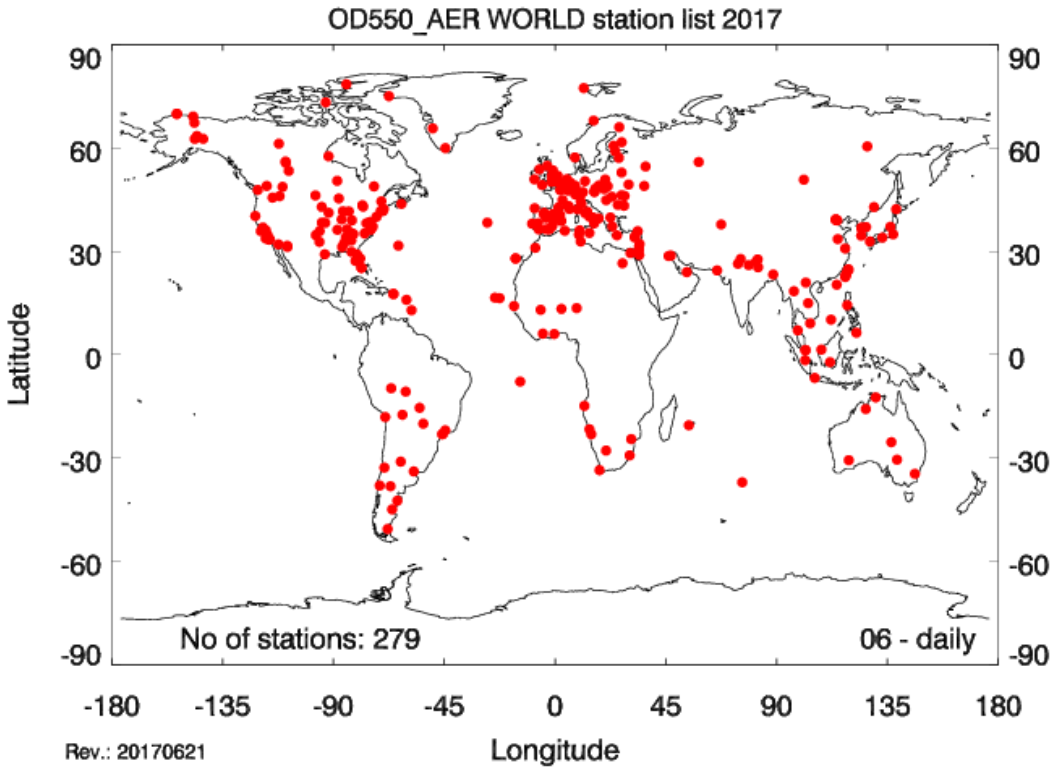

Figure 9.1: Sites with sun photometers reporting version 3 level 1.5 Aeronet data in June 2017.

way be compared to other model simulations, such as earlier MACC model versions, the MACC reanalysis or the AeroCom Median from an international multi-model ensemble.

9.2 Method for comparison of AOD and DOD over Northern Africa, Middle East and Europe

For the NRT AOD Mediterranean validation, we used AOD observations at 550 nm from 42 AERONET sites whose locations are depicted in Figure 9.2. Cloud-screened direct-sun data (Level 1.5) between 440 and 870nm under cloud-free conditions are used. Quantitative evaluations of the modelled AOD are conducted. The AOD at 550 nm is derived from data between 440 and 870 nm following the Ångström's law. Because AERONET data are acquired at 15-min intervals on average, all measurements within ±90 min of the models' outputs are used for the 3-hourly evaluation.

3-hourly values of AOD from AERONET and CAMS model outputs are used to check the model performance. CAMS model outputs (total AOD at 550nm) are bilinear interpolated in the horizontal at the stations' location. Mean Bias (MB), Fractional Gross Error (FGE), Root Mean Square Error (RMSE), Person correlation coefficient (r), and the number of data (NDATA), averaged over the study period are computed for this objective. This set of statistics is being computed for each AERONET site over the Mediterranean (shown in Figure 9.2).

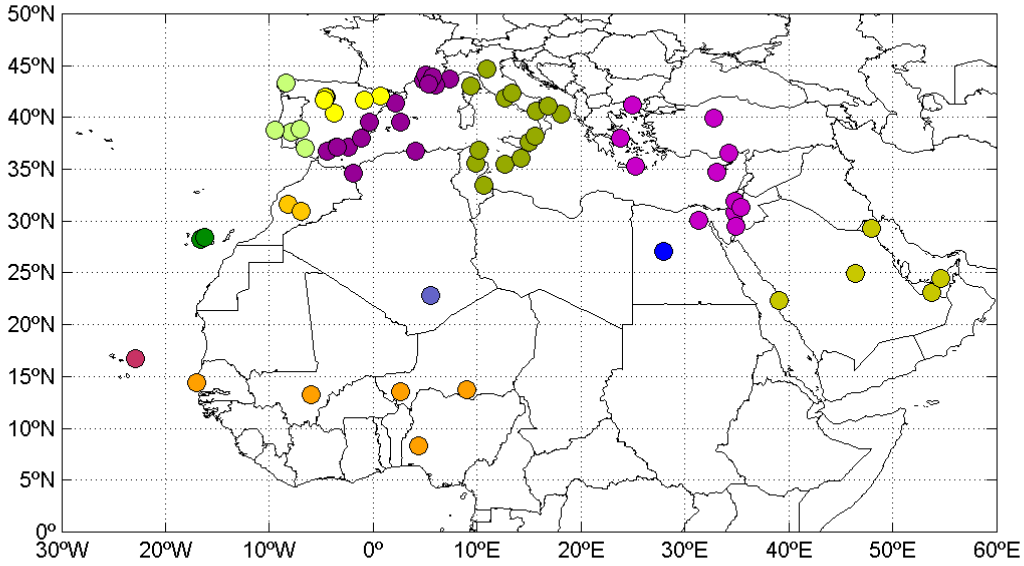

Figure 9.2: Map of 71 AERONET level-1.5 stations considered in the CAMS validation. The different colours distinguish regions.

The dust content is difficult to verify because bulk optical observations are not specific for dust. Since AOD is the degree to which a mixture of atmospheric aerosols prevents the transmission of light by absorption or scattering, we had to determine the criteria for filtering data in order to ensure that most of the AOD is influenced by mineral dust. Our first approach was to discriminate AOD observations clearly dominated by dust using Ångström's exponent (AE) as filter because it is inversely related to the average size of the particles: the smaller the particles are associated the larger AE. AE ranges normally from ~ 4 corresponding to molecular extinction to ~ 0 corresponding to coarse-mode aerosols (sea-salt and mineral dust) indicating a non-AOD wavelength dependence (O'Neill et al., 2003). Values of AE > 1.2 indicates significant presence of fine-mode particles (biomass burning or urban aerosols) (Basart et al., 2009). Quantitative evaluations of the modelled dust AOD (DOD) over North Africa-Middle East-Europe regional domain (whose locations are depicted in Figure 9.2) are conducted for dust-dominated conditions following Basart et al. (2009); i.e. when the AE≤ 0.75. All data with AE larger than 1.2 are considered free of dust (DOD = 0 is assumed). Values of AE between 0.75 and 1.2 are associated with mixed aerosols and are not included in the analysis. The AOD at 550 nm is derived from data between 440 and 870 nm following the Ångström's law.

In case of aerosol dust evaluation, a second methodology to discriminate DOD is being implemented. This second methodology is based in the fact that direct-sun AOD AERONET processing includes the Spectral Deconvolution Algorithm (SDA) retrievals (O'Neill et al., 2003). The SDA algorithm yields fine (sub-micron) and coarse (super-micron) AOD at a standard wavelength of 500 nm (AODfine and AODcoarse, respectively). However, the amplitude of the errors of the derived parameters varies as the inverse of the total AOD. In addition to measurement errors, there are errors in the AOD retrieval due to the uncertainty in the assumed values of the spectral curvature in each mode (O'Neill et al., 2001), which are most critical in coarse mode dominated conditions. Moreover, some of the AERONET sites have not been available the SDA Level 2.0.

According to Cuevas et al. (2015), by using the criterion of AODcoarse from the SDA retrieval, while the number of paired data points in the MACC-II-AERONET evaluation experienced no significant changes in the Sahara and the Sahel, this number grew significantly in other regions, especially in the dust transport corridors such as the Mediterranean regions, the North Western Maghreb and the Subtropical North Atlantic. Concerning long-range transport areas (i.e. North Atlantic and the Mediterranean), the AE filter applied to direct-sun AOD observations (AE < threshold value) just takes into account pure desert dust intrusions. Desert dust events in these regions are sporadic and consequently the number of observations is very low. The MNMB showed varying results, improving in some regions and worsens in others in comparison with direct-sun DOD observations (Cuevas et al., 2015). Summarizing both methodologies have advantages and disadvantages, depending on the region where DOD is evaluated.

Both methodologies to filter AERONET DOD will be used in CAMS DOD evaluation. CAMS model outputs (dust AOD at 550nm) are bilinear interpolated in the horizontal at the stations' location. 3-hourly values of DOD from AERONET and CAMS model outputs are used to check the model performance. Mean Bias (MB), Fractional Gross Error (FGE), Root Mean Square Error (RMSE), Person correlation coefficient (r), and the number of data (NDATA), averaged over the study period are computed for this objective. This set of statistics is being computed for each AERONET site and for 11 study regions (shown in Figure 9.2 by colours).

10 Method for comparison of DOD against Multi-model Median from SDS-WAS

The Sand and Dust Storm Warning Advisory and Assessment System (SDS-WAS) is a project of the World Meteorological Organization (WMO) with the mission to enhance the ability of countries to deliver timely and quality sand and dust storm forecasts, observations, information and knowledge to end users. The Regional Center for Northern Africa, Middle East and Europe (hereafter RC NAMEE or RC, http://sds-was.aemet.es/), hosted by the State Meteorological Agency of Spain (AEMET) and the Barcelona Supercomputing Center (BSC-CNS), supports a network of research and operational partners implementing the objectives of the SDS-WAS program in the region.

The DOD multi-model Median SDS-WAS product is obtained on a daily basis from the dust prediction models participating on the SDS-WAS model intercomparison (see the latest list of the model in the following link: http://sds-was.aemet.es/forecast-products/dust-forecasts/), which are downloaded from the Sand and Dust Storm Warning Advisory and Assessment System (SDS-WAS) Regional Center for Northern Africa, Middle East and Europe (see Figure 10.1). The dust model products exchange includes forecasts of dust optical depth at 550 nm (DOD) with lead times up to 72 h, based on 00 UTC or 12 UTC runs. The output frequency is of 3 hours. The model outputs are bi-linearly interpolated to a common grid mesh of 0.5º x 0.5º to create the DOD multi-model Median SDS-WAS product. More details of the generation of the SDS-WAS multi-model products can be found in the following link: http://sds-was.aemet.es/forecast-products/dust-forecasts/multimodel-products.

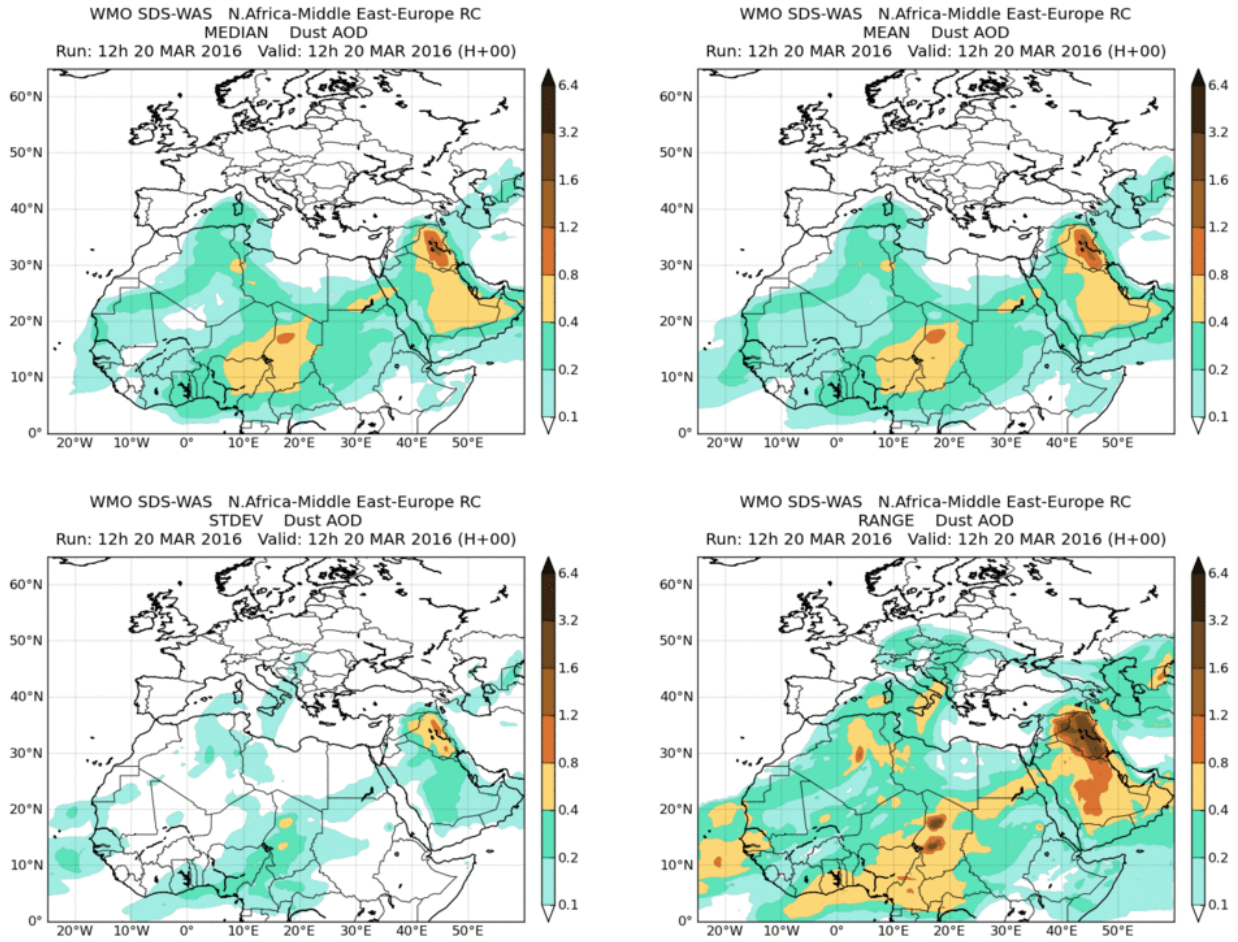

Figure 10.1: The DOD multi-model Median SDS-WAS product for 20 March 2016 at 12UTC (http://sds-was.aemet.es/forecast-products/dust-forecasts/multimodel-products)

11 DWD network ceilometers

11.1 DWD Ceilometer network

The German Meteorological Service (DWD) operates more than 110 CHM15K ceilometers as cloud base height monitors and aerosol profilers in its synoptic observations network. The low-cost/low-power elastic lidar systems, manufactured by Lufft (http://lufft.com – formerly by Jenoptik GmbH) evolved from cloud base height monitors into operational systems which allow to follow the planetary boundary layer (PBL) and aerosol layers in the free troposphere. With aid of nearby AOD measurements (Heese et al, 2010) or by absolute calibration (Wiegner et al., 2012) profiles of the particle backscatter or extinction coefficient can be inferred. The CHM15K uses a diode-pumped Nd:YAG solid state laser (1064 nm) and an off-axis Newton-type receiving telescope. Limited by the overlap between the laser beam and the telescope field of view, the signal can be used from about 0.4-10 km above ground with a vertical resolution of 15 m. For calibrated optical properties, the raw temporal resolution of 15s has to be averaged over at least 5 min.

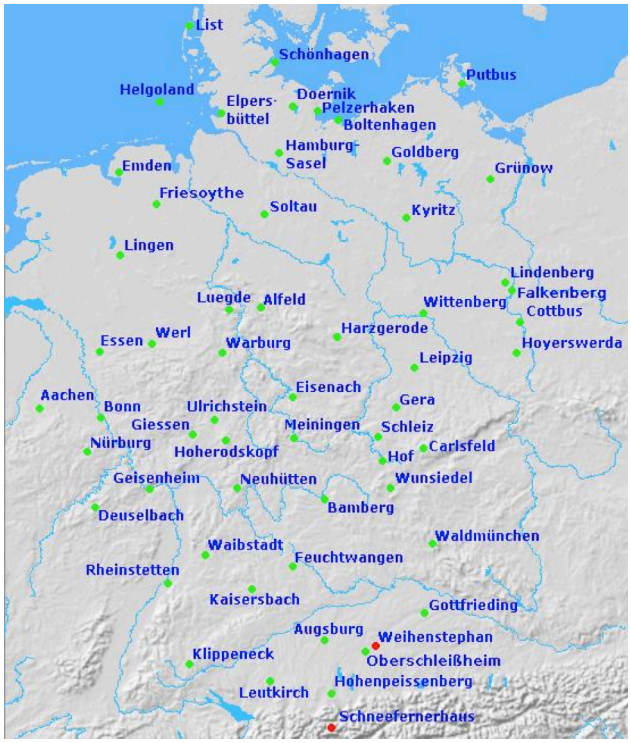

Ceilometer network of the German Meteorological Service (DWD)

11.2 (Attenuated) Backscatter Profiles

IFS data

Daily ncdf files with mass mixing ratios of the 11 prognostic aerosol variables, surface pressure, temperature, geopotential and boundary layer heights are retrieved from the MARS archive for both, the o-suite and the control run. The mass mixing ratios are converted to (attenuated) backscatter coefficients ($m^{-1}sr^{-1}$ or $(Mm)^{-1}sr^{-1}=10^{-6}m^{-1}sr^{-1}$) as follows: First, mass mixing ratios m, [kg/kg] are converted to mass concentrations c_m [kg/m^{-3}] by multiplication with air density, which is calculated from pressure and temperature. The extinction coefficient α, [m^{-1} or $(Mm)^{-1}=10^{-6}m^{-1}$] of each aerosol type is calculated by multiplying the mass concentrations with pre-calculated specific mass-extinction ratios σ^*_e, [m^2/g], depending on wavelength and relative humidity. The contribution of molecular scattering is considered using the Rayleigh formula. The backscatter coefficients β, [$m^{-1}sr^{-1}$] are finally obtained by dividing the extinction coefficients of each aerosol type by the respective lidar ratios S, [sr]. The attenuated backscatter coefficient

$\beta^*(r) = \beta(r)exp\{-2\int_0^r \alpha(r')dr'\} = \frac{Pr^2}{C_L}$, [$m^{-1}sr^{-1}$] is the backscatter coefficient degraded by the extinction between ceilometer and altitude r, whereby $\beta=\beta_m+\beta_p$ and $\alpha= \alpha_m+ \alpha_p$ are each composed of the molecule and particle contributions, and C_L is the lidar constant. The total backscatter coefficient is the sum of the individual aerosol types' backscatter coefficients.

The calculations of the conversion factors from mass to optical properties are based on Mie Theory. Refractive indices of the 11 aerosol types and their humidity dependency, their densities, specific mass-backscatter ratios and lidar ratios were extracted from the IFS aerosol code of LOA/LMD-Z or the respective auxiliary files. Where we were missing information, we calculated them with literature values taken from Boucher and Anderson (1995), Köpke et al. (1997), O'Dowd et al. (1997) Reddy et al. (2005) using the OPAC/GADS software package and database as in the IFS to ensure consistency (Morcrette et al, 2008, 2009).

The mass → backscatter conversion should better be a post-processing step at ECMWF ((attenuated) backscatter stored in MARS). Handling of the corresponding regional model output has still to be defined.

Table 11.1. Parameters requested from the ECMWF archive.

ECMWF-IFS aerosol optical (@1064 nm) and MARS-request parameters, if specified @ 70, 80, 90% rh.

Prognostic Variable	MARS -ID	Refr-Index	ρ [g/cm³]	σ^*_e [m²/g][B]	LR
DUST (0.03-0.55 µm)	4.210	1.48 + 6·10⁻³i (*)	2.61	2.6321 1.49(*)	78(*)
DUST (0.55-0.9 µm)	5.210			0.8679 1.61(*)	48(*)
DUST (0.9-20 µm)	6.210			0.4274 0.44(*)	13(*)
Hydrophilic BLACK CARBON	10.210	1.75 + 0.45i (*)	1.00	9.412	168(*)
Hydrophilic ORGANIC MATTER(#)	8.210	Bio: 1.44+0.001i(K) Anth: 1.55+0.001i(K)	1.769	5.502(#) 1.9/2.5/4.3(*)	46/49/57(*)
Hydrophobic BLACK CARBON	9.210	1.75 + 0.45i (*)	1.00	9.412	168(*)
Hydrophobic ORGANIC MATTER(#)	7.210	Bio: 1.44+0.001i(K) Anth: 1.55+0.001i(K)	1.769	5.502(#) 1.9/2.5/4.3(*)	46/49/57(*)
SEA-SALT (0.03-0.5 µm) (#)	1.210	1.51 + 2·10⁻⁴i (40%, SR) 1.42 + 4·10⁻⁵i (80%, SR) 1.36 + 5·10⁻⁸i (**)	1.183	3.0471 2.1/3.2/4.9(*)	65/76/73(*)
SEA-SALT (0.5-5 µm) (#)	2.210			0.3279 0.47/0.57/0.79	15/15/18(*)
SEA-SALT (5-20 µm) (#)	3.210			0.0924 0.13/0.15/0.21	15/15/9.5
SULPHATE(#)	11.210	1.60 + 0.0i (40%, SR) 1.44 + 0.0i (80%, SR)	1.769	6.609 2.6/3.5/6.0(*)	45/49/56(*)
CO	123.210	H2O, gas absorptions assumed t.b. negligible @1064 nm			
O3	203.210				
NO	27.217				
NO2	121.210				

(*) from LOA/LMD-z FTN code of O. Boucher
(SR) from S. Remy (ECMWF) for λ = 1.064 or 1.1 µm
(**) from Levoni et al, Appl. Optics, 36,30,1997
(B) from Benedetti et al, 2009
(#) depends on r.h.,
(K) valid for 532 nm Kim & Paulsen, ACP,13,7711ff, 2013 and to Nakayama et al, JGR,120,15,2015 (Imag-part), real-part with moderate wavelength dependence, imag-part strongly increasing with wavelength

Table 11.2. German Ceilometer stations.

Station	lat	lon	alt	Station	lat	lon	alt	Station	lat	lon	alt
list	55.01	8.41	26	lindenberg_	52.21	14.12	123	meiningen	50.56	10.38	450
leck	54.79	8.95	7	lindenberg	52.21	14.13	101	hoherodskopf	50.51	9.22	743.3
schoenhagen	54.64	10.02	2	falkenberg	52.17	14.12	73	carlsfeld	50.43	12.61	897
schleswig	54.53	9.55	43	magdeburg	52.1	11.58	85	nuerburg	50.36	6.87	485
putbus	54.37	13.48	39.5	alfeld	51.97	9.8	143.9	hof	50.31	11.88	565.1
st-peter-ording	54.33	8.6	5	wittenberg	51.89	12.65	105	wunsiedel	50.03	11.97	622.3
helgoland	54.18	7.89	4	Luegde	51.87	9.27	258	neuhuetten	50.01	9.43	339.5
doernick	54.17	10.35	26.3	wernigerode	51.85	10.77	240	geisenheim	49.99	7.95	110.2
pelzerhaken	54.09	10.88	1	cottbus	51.78	14.32	69	bamberg	49.88	10.92	240
elpersbuettel	54.07	9.01	3	harzgerode	51.65	11.14	404	deuselbach	49.76	7.06	480.5
boltenhagen	54	11.19	15	doberlug	51.65	13.58	100	waldmuenchen	49.39	12.69	498.8
quickborn	53.73	9.88	14	werl	51.58	7.89	84.8	waibstadt	49.3	8.91	236.6
norderney	53.71	7.15	11	warburg	51.51	9.11	235.8	berus	49.28	6.63	363
hamburg	53.65	10.11	35	hoyerswerda	51.45	14.25	115.9	feuchtwangen	49.16	10.37	475.1
goldberg	53.61	12.1	58	essen	51.41	6.97	150	rheinstetten	48.97	8.33	116.1
waren	53.52	12.67	70	leipzig	51.32	12.45	138	kaisersbach	48.92	9.69	488.7
emden	53.39	7.23	0	kahlerasten	51.18	8.49	839	gottfrieding	48.66	12.54	350.4
gruenow	53.32	13.94	55.9	goerlitz	51.16	14.96	240	augsburg	48.43	10.94	461.4
friesoythe	53.05	7.9	5.7	eisenach	51	10.36	312.4	weihenstephan	48.4	11.7	477.1
soltau	52.96	9.8	75.6	gera	50.88	12.13	311	oberschleissheim	48.24	11.55	484
kyritz	52.94	12.41	40	aachen	50.8	6.03	231	klippeneck	48.11	8.76	973.4
lingen	52.52	7.31	22	chemnitz	50.79	12.87	420	schauinsland	47.91	7.91	1205
genthin	52.39	12.16	35	ulrichstein	50.75	9.02	350.3	hohenpeissenberg	47.8	11.01	977
potsdam_alt	52.38	13.06	81	bonn	50.74	7.19	159	leutkirch	47.8	10.03	671.7
potsdam	52.38	13.06	81	schmuecke	50.66	10.77	948	hohenpeiss-ICOS	47.8	11.01	992
lindenbergtest	52.3	14.12	115	giessen	50.6	8.65	202.7	garmisch	47.48	11.07	719
braunschweig	52.29	10.45	81	schleiz	50.57	11.81	501	schneefernerhaus	47.42	10.97	2650

Aerosol representation in the IFS model

The 11 prognostic aerosol types, handled by the IFS model, are described in Morcrette et al. (2008, 2009), but the treatment of humidity deserves particular attention. The IFS model transports and provides aerosols in the dry state, but at each time step grows them according to relative humidity in order to calculate the relevant optical properties in the cases of sulphate, hydrophilic organic carbon and sea salt. (Though there is 'hydrophilic black carbon', its optical properties are not distinguished from those of the hydrophobic fraction.) However, no interaction of the humidity dependent growth with microphysical processes, no re-distribution between size bins (i.e. physical growth due to water uptake) nor chemical or phase transformations is taken into account. The output fields are valid for the very time of output and at the model grid point, i.e. no temporal or spatial averaging is included.

Ceilometer Data

Daily ncdf files with profiles every 15s from >110 German stations are operationally stored as Pr^2 (=range-corrected intensity) by DWD (cf. table 11.2). These data are averaged to hourly means (nc-operators) and converted to (attenuated) backscatter ($Pr^2 \rightarrow \beta^*$) with aid of calibration constants (C_L: $\beta^*_{,ceilo\text{-}x}=Pr^2 \cdot C_{L,ceilo\text{-}x}$), which are regularly determined/updated for each instrument under favourable conditions. Initially, only stations are selected for evaluation which are less than 20 km distant from a model grid point and whose real altitudes correspond to the model orography (surface level 60) within Δalt<100m in order to avoid vertical re-sampling issues. No averaging of ceilometer data over stations is performed for continuity reasons. The calibration constant C_L contains all system-specific parameters, occurring in the elastic lidar equation, such that the received power can directly be related to the attenuated backscatter coefficient β^* ($P=C_L*1/r^2*\beta^*$, where the usual attenuation term exp{-2·AOT} is omitted).

Horizontal and vertical interpolation/resampling (draft)

Horizontally: Yet no interpolation of model profile from nearest grid-points to stations' locations. This needs further discussion!

Vertically: Level altitudes (above model orography – L60) are calculated as barometric height, based on surface pressure p_s and sigma-hybrid-coefficients a_k, b_k: $p_k(n,j,i) = a_k + b_k*p_s(n,j,i)$ (for level centres). Then ceilometer profiles are simply resampled at the model levels without interpolation or application of any averaging kernels. Until the handling of stations, where model orography deviates significantly from real altitude, is clear, these are excluded.

Uncertainties (draft)

Ceilometers: Error of the ceilometers' β^*–profiles is composed of contributions from SNR and calibration (no assumptions about particles required for β^* – only on instrument stability). Absorptions can be neglected at the 1.064µm wavelength. Laser degradation, ageing of the optical components, pollution or snow on the output window 'only' reduces the SNR, but miss-alignment and other malfunctions can lead to not quantifiable errors in the operational (24/7) instruments. Usually $\Delta\beta^*_n \approx$20-50% can be reached under favourable atmospheric conditions. No measurement is possible above/beyond beam blocking clouds, during strong precipitation or fog.

Model: Here largest evaluation uncertainties arise from synchronization/co-location, particularly in the vertical, strong gradients in presence of temporal or spatial shifts, the conversion of physical to optical quantities, dynamics, etc. (model uncertainty estimate based on AN/FC covariance or from assimilation).

11.3 Boundary layer heights (BLH)

ECMWF data

The planetary boundary layer height (or mixing layer height) z0 is retrieved from MARS to daily ncdf-files by cronjob, both for o-suite and ctrl. The FC steps 0,3,6,9,...,21 are based on the daily 00 UT analysis. The IFS model associates the BLH with a certain value (0.25) of the bulk Richardson number, which characterizes the degree of turbulence. The vertical stability is estimated using the difference between a level and the lowest level. Several issues with this approach are described by e.g. v. Engeln and Teixeira (2013), related to the Richardson number being based on ratios of both dynamic and thermodynamic vertical gradients rather than of temperature and/or humidity as such, the use of dry varis in cloudy situations, and the fact that the Richardson number as a measure of local turbulence is often unable to properly characterize the turbulent properties of convective boundary layers. Turbulent kinetic energy, which could better be used, however, is rarely used in global models and as such is not available (v.Engeln and Teixeira, 2013). CAMS model level geopotential heights are used to characterise the model-station height difference.

Ceilometer data

The BLH observations are taken as provided by the firmware, implemented in the CHM15k ceilometers. It is calculated from the backscatter intensities of the ceilometer range corrected signal (Pr2) by means of a wavelet transform algorithm, developed by Teschke and Pönitz (2010). In principle, the BLH detection is a pattern recognition problem, which is based on the assumption that the vertical distribution of aerosol can be used as a tracer for boundaries. This, however, is not always the case. The absolute value of the backscatter is typically not needed since the relevant information seems to be completely coded in the gradient (but possibly of different orders) of the backscatter profile (Teschke and Pönitz, 2010). Up to 3 layers are reported, the highest of which is identified with the top of the convective ML during daytime and the lowest one to the stable BL at night-time. Haeffelin et al. (2012) investigated limitations and capabilities of existing mixing height retrieval algorithms by comparing different retrieval techniques. They found "no evidence that the first derivative, wavelet transform, and two-dimensional derivative techniques result in different skills to detect one or multiple significant aerosol gradients" (Haeffelin et al., 2012). Generally, there is no perfect way to determine the height of the ML, both in observations and models, and the appropriateness of each method depends on the topic being investigated. The inferred MH may not be realistic in cases with multiple layers, low clouds/fog, missing aerosol gradients, precipitation and intense long-range transport of e.g. Saharan dust. These data can be rejected according to spatial inhomogeneity or temporal discontinuity. For a first approximation, if data are missing due to meteorological conditions or are spurious at individual stations, these are disregarded by discussing median MLH instead of means.

Uncertainties

From the 3 BLH, reported by the CHM15k-Nimbus, simply the uppermost is used. Since yet no quality or plausibility flag is available, the uncertainty cannot be quantified. Thus the evaluation is semi-quantitative, only, but yields significance through using median values instead of means.

12 Contribution from NDACC

NDACC is a cross-border international research network of remote sounding stations (Fig. 12.1 and 12.2). It is a major contributor to the World Meteorological Organisation (WMO) GAW programme and it works under the auspices of United Nations Environment Programme (UNEP) and the International Ozone Commission (IO3C). Relying on a strong involvement of European partners and efficient collaboration with partners worldwide, the network started operations officially in 1991, but a few data records extend back to the 1970s and even to the 1950s. At present time it includes more than 70 high-quality, remote-sensing research stations/sites distributed worldwide for (i) observing and understanding the physical / chemical state of the stratosphere and troposphere, and (ii) assessing the impact of stratospheric changes on the underlying troposphere and on global climate.

Validation of CAMS model data using observations from the NDACC network (ndacc.org) for a selected number of instruments (see below) was developed during the NORS EU project (Demonstration Network Of ground-based Remote Sensing observations in support of the Copernicus Atmospheric Service, EU FP7 project) (De Mazière et al., 2012, 2013), see http://nors.aeronomie.be and nors-server.aeronomie.be. The instruments used are

- Fourier Transform InfraRed (FTIR)
- MicroWave Radiatiometers (MWR)
- UV-Visible Differential Optical Absorption Spectroscopy (DOAS) and multi-axis DOAS or MAXDOAS
- Differential Absorption Lidar Technique (LIDAR)

For more information on the different instruments, see http://www.ndsc.ncep.noaa.gov/instr/. For a detailed description of each measurement technique, retrieval methods, reported uncertainties, data processing and filtering is found in the NORS data user guide deliverable http://nors.aeronomie.be/projectdir/PDF/NORS_D4.2_DUG.pdf. Below a brief description is found per instrument technique and the typical measurement uncertainties.

Presently the NORS server validates O_3 using FTIR, MWR, UVVIS DOAS and LIDAR measurements, CO and CH4 using FTIR measurements, tropospheric H_2CO, NO_2 and aerosol using UVVIS DOAS and stratospheric NO_2 using FTIR measurements (the latter is not fully harmonized on NDACC). The validation server is able to work with any target species available on NDACC for any of these instruments, see Figure 12.3.

All NDACC available stations submitting data in the GEOMS HDF file format are used in the validation server (nors-server.aeronomie.be). There is no a-posteriori data filtering for the NRT validation reports, apart from an obvious filtering on corrupted NDACC data.

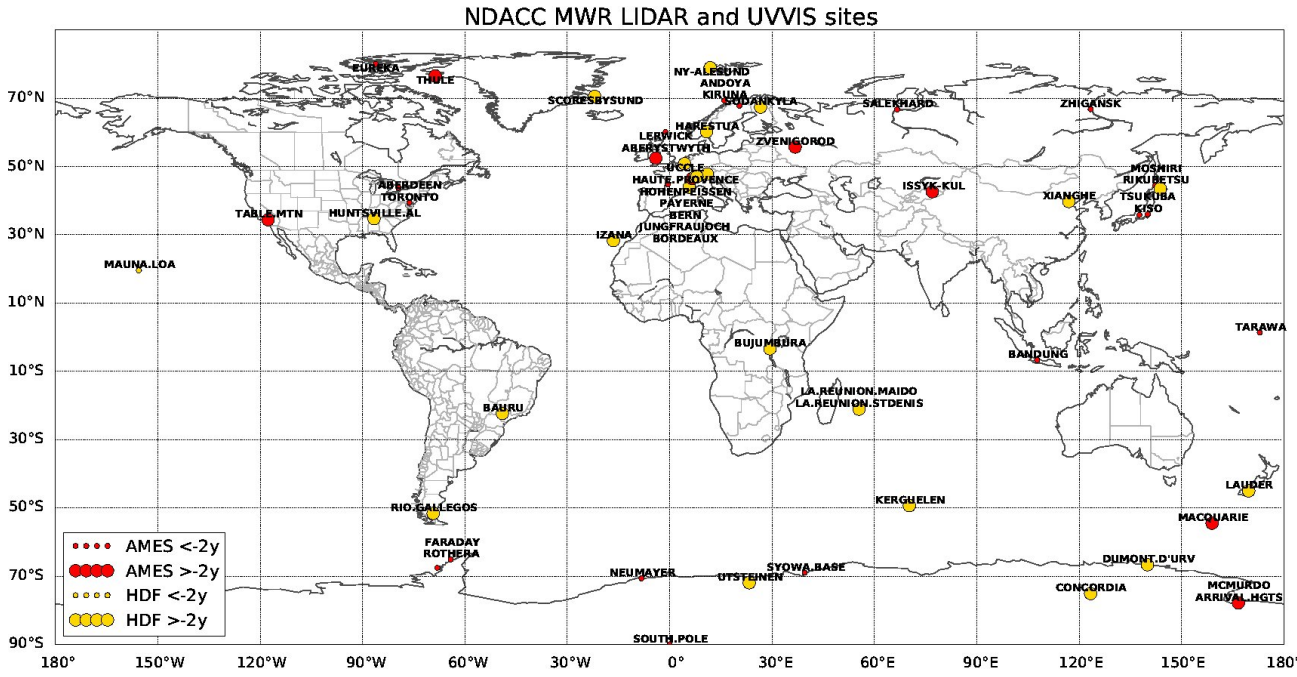

Figure 12.1: NDACC stations for LIDAR, MWR and UVVIS. Stations submitting HDF (ready for use in CAMS84) are indicated in yellow. Red stations submit data in ascii AMES format: stations submitting recent AMES data may be of potential use for CAMS84 (stations that have not submitted data in the past two years (<-2y) are shown with a small green circle.).

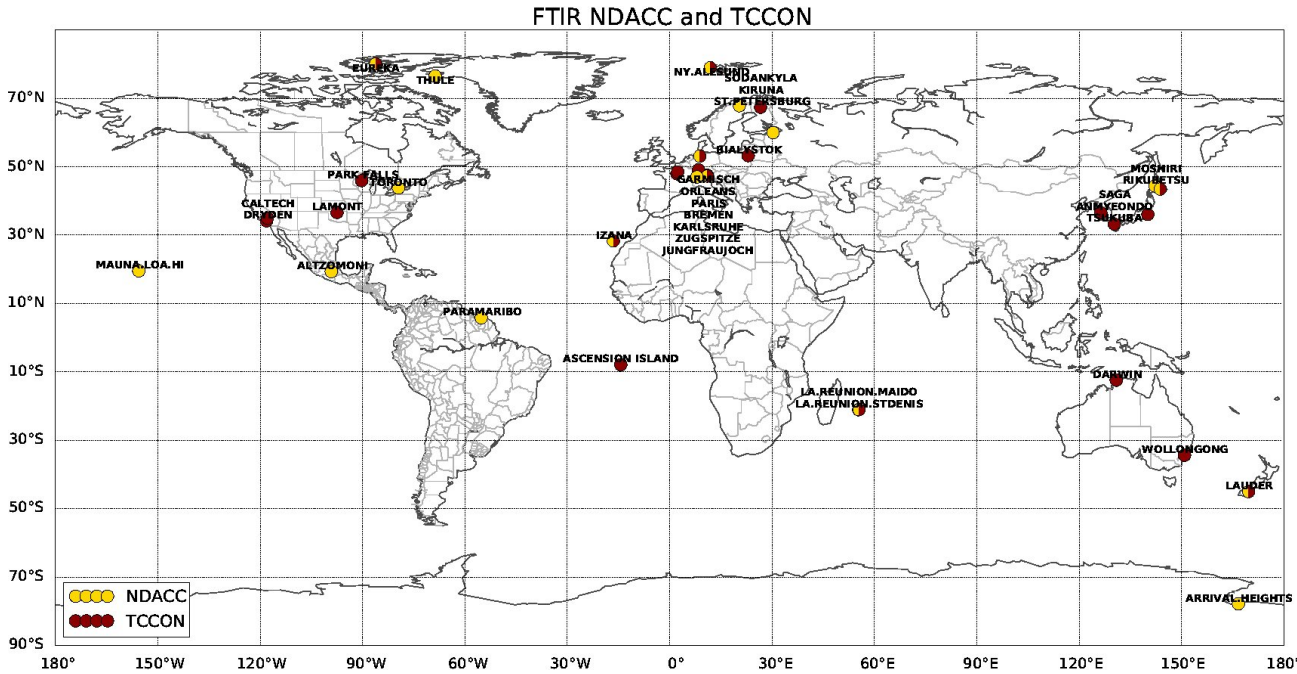

Figure 12.2: NDACC FTIR stations (yellow) submitting data in HDF format; TCCON stations are indicated in red (some stations measure for both TCCON and NDACC). The TCCON stations at Reunion, Orleans and Bialystok submit data in Rapid Delivery mode.

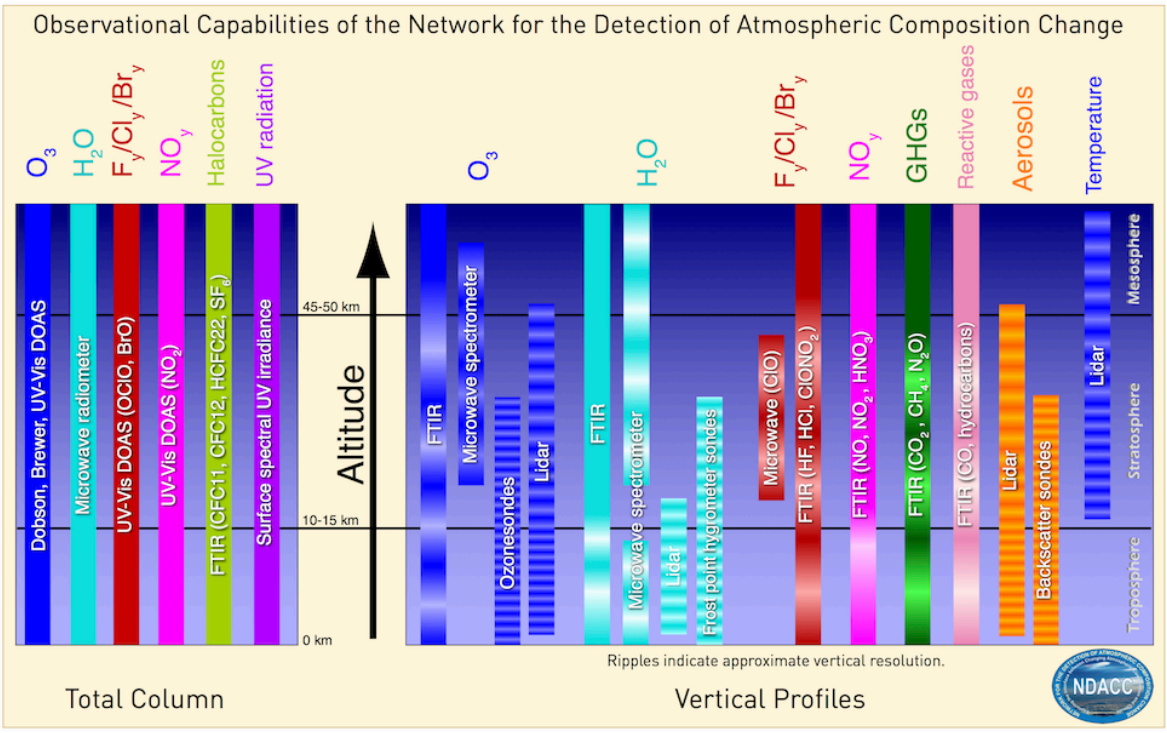

Figure 12.3: Overview of NDACC observational capabilities (picture taken from http://www.ndsc.ncep.noaa.gov).

Measurements are validated against model data if the difference between the measurement time and validity time of the model data is not greater than a pre-defined threshold value (1/2h for MWR O_3 and UVVIS H_2CO measurements, 3h for NDACC all FTIR measurements except NO_2 (1/4h) and TCCON data (1/3h), etc.) according to the variability of the measured species and availability of the data. Using the model vertical pressure grid and the model geopotential surface height, a vertical height grid for the model is constructed. Next, a model profile is obtained at the sites location using a bilinear interpolation for the surrounding model grid points (for FTIR measurements, the model profile is extracted along the line of sight).

The target model data is regridded to the measurement vertical grid using a mass-conserving interpolation (i.e. layer height weighted regridding for number density profiles). Finally the regridded model profile is smoothed using the averaging kernels (except for O_3 LIDAR measurements, where smoothing is not applicable); see below for some example kernel matrices. From this smoothed model profile the desired partial columns are calculated and compared against the measurements. A detailed description of the validation methodology is described in Langerock et al (2014).

12.1 Validation with Microwave radiation measurements (MWR)

Microwave radiation measurements use a FFT spectrometer to record the pressure- broadened ozone line spectra at 142 GHz with a bandwidth of 1 GHz. Measurements are available every 30' and sensitivity typically start at 25km.

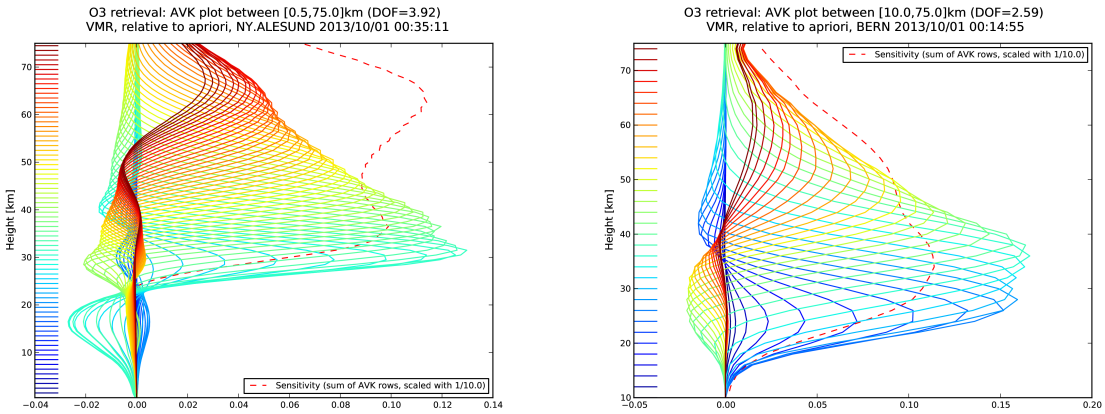

Figure 12.4: Typical averaging kernels for the Ground-based MWR stations of the NDACC network: sensitivity lies between ±20km and ±80km.

Figure 12.4 shows typical averaging kernels and from the measurement's sensitivity (dashed red line). In the validation, the profile comparisons are restricted to an altitude range between 20 and 60km: above and below this height range the instrument has no sensitivity or the model does not provide data. The typical uncertainty for the stratospheric columns is 5-10% (Hocke, 2007; Kämpfer, 2013; Peter, 1997).

12.2 Validation with Fourier Transform InfraRed measurements (FTIR) from NDACC and TCCON

FTIR measurements of O_3, CH_4, CO_2 and CO are taken by a Michelson-type interferometer, looking directly at the centre of the sun (or moon). The FTIR NDACC data does not contain CO_2, and TCCON CH_4, CO and CO_2 data used in CAMS validation reports.

The validation of the model data against these observations is basically the same as for MWR measurements. The only difference is that for FTIR measurements, model data are validated against measurements that are within an interval of one time step around the time of model output.

The NDACC FTIR data consists of total columns (mol/cm^2), as well as VMR and partial columns (mol/cm^2) per atmospheric layer defined on a height grid (km). The averaging kernel illustrate that these FTIR instruments can only be used up to +/-60km, as the instrument has only little or no sensitivity above. Measurement uncertainties are site and target dependent, and typically range from 5-10% (ISSI, 2012).

TCCON FTIR data consists of dry air averaged columns (xgas, mol/mol) only. TCCON reports a column averaging kernel and the smoothing equation transforms the model profile to a column value. The precision for CH4 is approximately 0.3%, for CO 1% and for CO2 the precision is 0.25%.

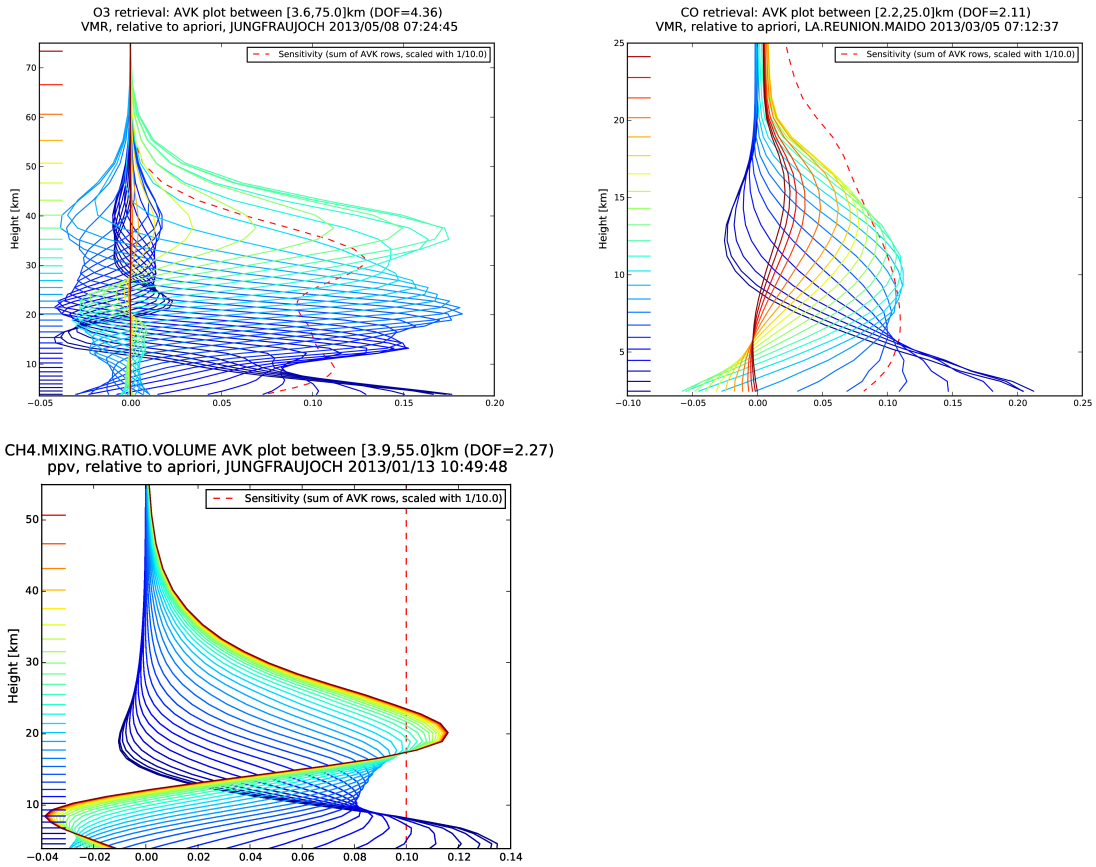

Figure 12.5 Example of AVK's in VMR/VMR units for ozone (left top) and CO (right) and methane (bottom). The dashed curve in the right plot represents the sensitivity curve, which vanishes at between 50 and 60km for ozone. CO measurements are sensitive up to 25km.

12.3 Validation with NO2, O3, H2CO and Aerosol UVVIS DOAS measurements

In a Multi-AXis or MAX-DOAS instrument, light is guided into the spectrometer by a telescope that can be pointed at the sun or at different parts of the sky. Depending on the instrument and application, different operation modes can be used:

1. Zenith sky operation for total columns, stratospheric profiles and tropospheric columns with low sensitivity

2. Direct sun operation for total columns and in combination with scattered light observations for atmospheric profiles

3. Multi-Axis operation with multiple viewing directions above the horizon for tropospheric profiles and (if azimuthal pointing is possible) horizontal gradients.

UVVIS (MAX-)DOAS ((Multi-Axis) Differential Optical Absorption Spectrometer) measures scattered sunlight at different elevation angles above the horizon. Measurements are sensitive to clouds and provide good tropospheric profile under homogeneous cloud conditions see Gielen et al., (2014). UVVIS DOAS (zenith measurements) also measure stratospheric O_3 and NO_2, which are column only

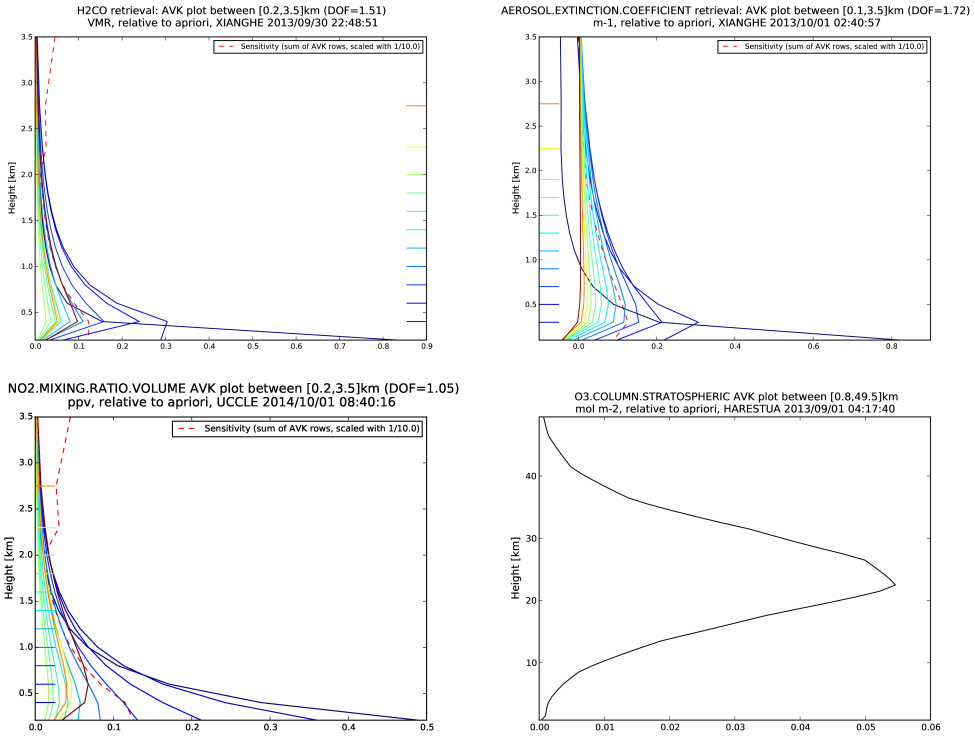

Figure 12.6. A typical UVVIS DOAS OFFAXIS AVK for H_2CO and NO_2 (VMR/VMR) and Aerosol extinction profile (m^{-1}) retrievals. The measurement is sensitive below 1km. For the UVVIS ozone zenith sky measurements (only column data) the column AVK is shown.

data. Uncertainties are site and target dependent and may range from 5-10-20% (Clemer et al., 2010; Connor et al., 1994; Eskes and Boersma, 2003; Frieß et al., 2006).

12.4 Validation with Light Detection And Ranging measurements (LIDAR)

LIDAR measurements used in this report were also collected in the framework of the NORS project (http://nors.aeronomie.be). The lidar (Light Detection And Ranging) technique (http://ndacc-lidar.org/) is a remote sensing measurement technique using the scattering properties of light by gases, liquids, and solids in order to infer their physical or chemical properties (Godin et al., 1994; McGee et al., 1993). A laser beam is sent into the atmosphere. The light is scattered by the atmospheric molecules and particles, and a fraction is collected back on the ground with a telescope. Since the lidar comprises the light source itself, the lidar technique is known as an 'active remote sensing' technique.

There are currently 30 lidar instruments worldwide contributing to NDACC. These instruments use three different lidar techniques to retrieve atmospheric temperature, ozone and aerosol properties:

- typically 30-80 km, down to 10 km if using Raman channels
- typically 20-40 km
- typically 10-45 km in the stratosphere, 1-10 km in the troposphere

Because the transition from L1 to L2 data is not based on optimal estimation, the measurement data does not contain AVK and no smoothing is applied to the model profile. To align the number density profiles of both model and measurement, a mass-conserving regridding technique is used. For temperature, a layer thickness weighted mean is calculated to convert the lidar profile to the coarser model grid. The typical uncertainty on the partial column data 15km<45km is 3% and, the profile NB uncertainties range from ~1% at 20km to 30% at 50km.

13 Limb-scanning satellite instruments

13.1 Validation with OMPS-LP observations of O_3

The Ozone Mapping and Profiler Suite (OMPS) is composed of three instruments aboard Suomi National Polar-orbiting Partnership (S-NPP) satellites: the Nadir Mapper (OMPS-NM), the Nadir Profiler (OMPS-NP) and the Limb Profiler (OMPS-LP).

For the validation of the CAMS stratospheric ozone product, we use the level 2 daily retrievals from the OMPS-LP instrument (LP-L2-O3-DAILY product), release 2. This dataset starts on 10 February 2012 and is currently delivered in NRT with a latency of about 5 days at https://ozoneaq.gsfc.nasa.gov/data/omps/.

The OMPS-LP instrument has been designed to allow retrievals of ozone concentration profiles from the tropopause up to 60km. It views the Earth's limb looking backwards along the orbit track, using three parallel vertical slits. One slit is aligned with the orbit track, and the other two slits are pointed 4.25° to each side, giving an effective cross-track separation of approximately 250 km at the tangent point. Each profile corresponds to along-track sampling of approximately 125 km (Jaross et al. 2012).

According to a performance evaluation (Jaross et al., 2014), it is noticed that the Limb instrument operates mostly as designed and basic performance meets or exceeds the original design criteria.

The initial version of LP-L2-O3-DAILY (release 1) has been replaced by a new version (release 2) in July 2014, with several changes. Preliminary results of comparison of this release with AURA MLS (Xu et al. 2014) show a good agreement: "… an example of the results obtained when we compare LP ozone data with MLS ozone data for a monthly average in February 2014. Zonal mean differences are generally less than ±10% between 10 km and 60 km over all latitudes, with some larger differences only below 20 km in the tropics." However, some consistent differences between results from the three slits are noted: left slit ozone values are typically 5-10% higher than centre slit values above ~40 km, and are ~10% lower between 15-20 km in the tropics. Similarly, right slit ozone values are typically 5-10% lower than centre slit values above ~40 km, and are ~10% higher between 15-20 km in the tropics. There is no clear evidence of which slit may give the most accurate absolute results.

In the LP-L2-O3-DAILY product, separate retrievals are performed (for overlapping altitude ranges) using radiance data at ultraviolet (UV) and visible (VIS) wavelengths, and a combined ozone profile (VIS retrieval between 0-26.5 km, UV between 27.5-60.5 km) for each event is created from these individual retrievals. Note that no merging procedure is applied for the combined profile; these discontinuities are clearly visible in profiles in the northern latitudes. Approximately 6500 valid profiles are generated daily, within a latitude range of 85° South to 85° North. Each profile is also reported in mixing ratio format on a regular pressure grid. To this end, the retrieval uses temperature and pressure profiles from NASA Global Modelling and Assimilation Office (GMAO) GEOS-5 FP-IT Np gridded data (on 42 pressure levels up to 0.1hPa, at 0.5° latitude x 0.625° longitude horizontal resolution, every 3 hours). For each data value a precision value is reported based on the

estimated standard deviation derived from the diagonal of the covariance matrix of the optimal estimation solution for the retrieval.

The first step of the validation procedure consists in mapping the model data in the observations space.

The observations used for the validation are selected according to quality and usability criteria usually defined in accompanying documentations of the dataset. For the OMPS-LP LP-L2-O3-DAILY product, all the successfully retrieved O_3 volume mixing ratio on the pressure grid are used.

The model data are converted to volume mixing ratio, and interpolated along the time dimension. These interpolated data are mapped to the observation space by bilinear interpolation for the horizontal dimension and a vertical interpolation on the observations pressure grid. These model-at-observation (MAO) data, along with indicators of observation quality, are saved for further processing.

The second step of the validation builds statistics, in different latitude bands, on the observation datasets, the MAO datasets and their differences. The quality indicators in the datasets allow the selection of matching data in all datasets.

13.2 Validation with ACE-FTS observations of O_3

ACE-FTS is one of the two instruments on the Canadian satellite mission SCISAT-1 (first Science Satellite), ACE (Bernath et al., 2005). It is a high spectral resolution Fourier transform spectrometer operating with a Michelson interferometer. Vertical profiles of atmospheric parameters such as temperature, pressure and volume mixing ratios of trace constituents are retrieved from the occultation spectra, as described in (Boone et al., 2005) with a vertical resolution of maximum 3-4 km. Level 2 ozone retrievals (version 3.6) are used as an independent reference data set to validate the distribution of stratospheric ozone in the analyses and forecasts generated by CAMS.

It must be noted that the low spatio-temporal sampling of ACE-FTS (due to the solar occultation technique) does not deliver profiles in all latitude bands for each month. There are also two periods during the year where there are no measurements for a~duration of almost 3 weeks due to the fact that the spacecraft is in constant sunlight: June and December (Hughes and Bernath, 2012).

As shown on fig. 13.1, there are four periods per year, lasting about 1 month (northern hemisphere: April, June, August, December; southern hemisphere: February, June, October, December) with no occultation poleward of 60°. At very high β angles (i.e. the angle between the orbital plane of the satellite and the Earth-Sun direction > 57°), it is common practice to skip more than half of the available measurement opportunities to avoid exceeding onboard storage capacities and overlapping command sequences. Therefore, the amount of observations in the tropics is significantly lower than in the polar regions.

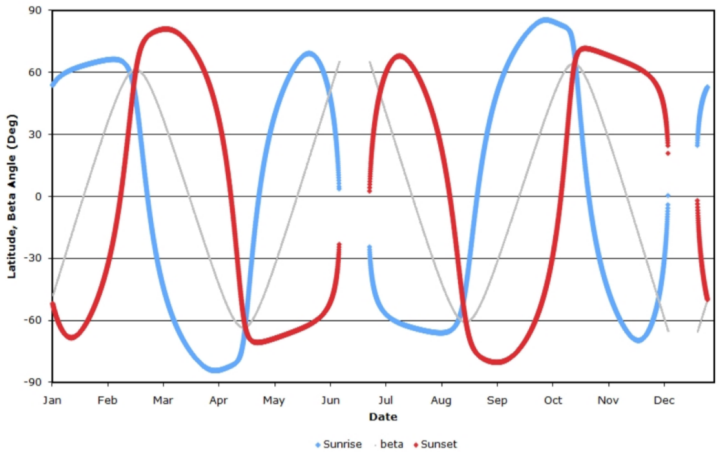

Figure 13.1. Occultation latitudes for ACE for one year on orbit. The red and blue lines indicate locations for sunrise and sunset occultations, respectively. The grey line shows the beta angle associated with the measurement. Note that by design, the latitudes of the ACE observations repeat every year, but the longitude of the occultations change from year to year. Copied from fig. 4 in Hughes and Bernath (2012).

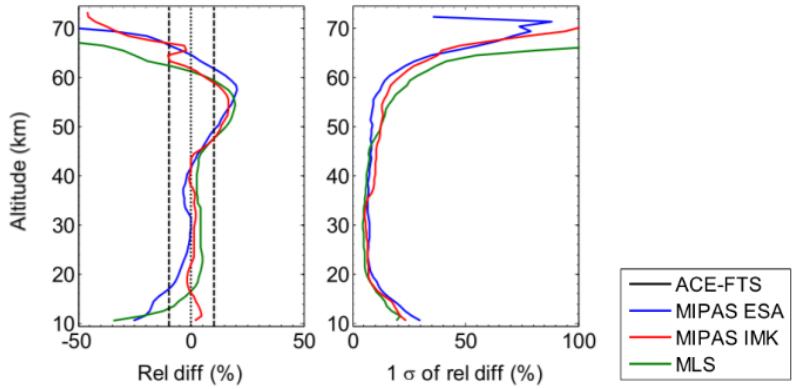

Figure 13.2. O_3 comparisons using coincidence criteria of within 3 h and 350 km. The left panel shows the mean of the relative differences (ACE-FTS minus other instrument) in percent, and the standard deviations of the relative differences in percent. Copied from fig. 2 in Sheese et al. (2017).

Teigtmeier et al. (2013) performed an intercomparison of ozone climatologies by satellite limb sounders including ACE-FTS (v2.2) and showed that the ACE-FTS climatology agreed well with those of the other instruments in the lower and mid-stratosphere but had a positive offset in the upper stratosphere. This was confirmed by Sheese et al. (2017) using a comparison of coincident ozone profiles between the latest version of ACE-FTS (3.5), Aura-MLS 3.3/3.4 (which is assimilated in CAMS o-suite and reanalysis) and MIPAS (which is assimilated in the CAMS reanalysis). The ACE-FTS data used as independent reference in CAMS-84 is typically within ±5% of mid-stratospheric MIPAS and MLS data and exhibits a positive bias of 10 to 20% in the upper stratosphere–lower mesosphere.

This comparison uses the quality flags newly added in ACE-FTS since v3, hence filtering out physically unrealistic outliers (at any altitude) and profiles were known to be affected by instrument or processing errors. These quality flags are also used for CAMS-84 validation.

ACE-FTS v3.6 ozone profiles are delivered with a latency of two days but the complete dataset with necessary quality flags are available only with ~45 days latency. The observations used for the validation are selected according to quality and usability criteria usually defined in accompanying

documentation of the dataset (Walker et al., 2017). For the ACE-FTS v3.6 product, all the O_3 volume mixing ratio successfully retrieved on the altitude grid are used. The pressure at each observation is interpolated from the model altitudes (i.e. based on the model temperature fields).

Since ACE-FTS has limited sampling, any comparison between climatologies shows large sampling errors. This explains the rather large negative offset in the polar regions between ACE-FTS and the Multi-Instrument Mean of the SPARC Data Initiative (Tegtmeier et al., 2013, fig.2). Sheese et al. (2017) also showed the large diurnal biases appearing in comparisons between ACE-FTS sunrise (sunset) and MIPAS/MLS daytime (nighttime) profiles.

The first step of the validation procedure consists in mapping the model data in the observations space: the model data are converted to volume mixing ratio, and interpolated along the time dimension using either the CAMS 6-hourly analyses or 3-hourly forecasts. These 3-D distributions are mapped to the observation space by bilinear interpolation for the horizontal dimension and a vertical interpolation on the observations pressure grid. Hence there are no sampling biases in CAMS-84 validation (see also Lefever et al., 2015).

These model-at-observation (MAO) data, along with indicators of observation quality, are saved for further processing. The second step of the validation builds statistics, in different latitude bands, on the observation datasets, the MAO datasets and their differences. The quality indicators in the datasets allow the selection of matching data in all datasets.

14 Greenhouse gas observations with TCCON

The Total Carbon Column Observing Network (TCCON), established in 2004, is a network of ground-based Fourier Transform Spectrometers that record spectra of the sun in the near-infrared. From these spectra column-averaged abundances of atmospheric constituents including CO_2, CH_4, N_2O, HF, CO, H_2O, and HDO, are retrieved. The final data product is column averaged mole fractions, denoted by the prefix "X". TCCON measurements are vital for

- the calibration of remote sensing data against the in situ reference scale and
- the validation of satellite retrievals.

In addition the TCCON data complements the surface stations data in a way that enables data-model fusion techniques (inverse modelling, assimilation) to reduce the spatial and temporal uncertainty of estimated sources and sinks of GHG. The TCCON was included in the Global Atmosphere Watch (GAW) of the WMO in 2009. Details about the network are given in Wunch et al. (2011).

Instruments that are currently accepted in the TCCON are the laboratory type spectrometers Bruker IFS 120HR and Bruker IFS 120HR, with CaF_2 beamsplitters and room-temperature DC-enabled InGaAs detectors. Desired, but not required are DC-enabled Si detectors for the O_2 A-band with dual-beam acquisition.

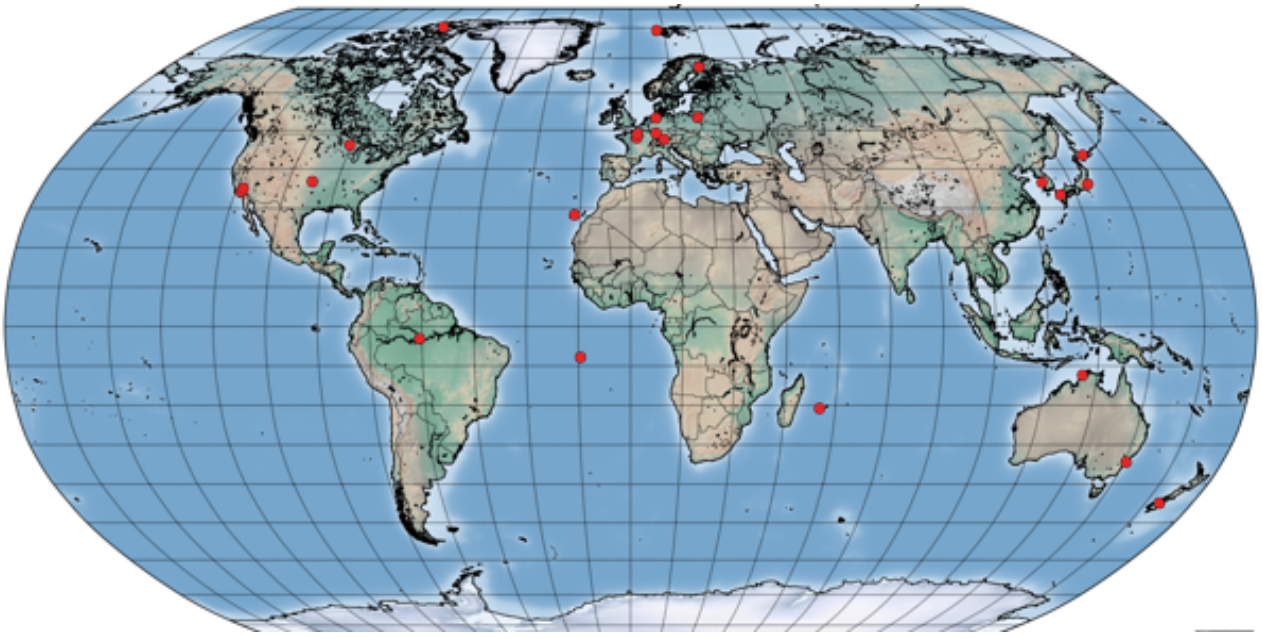

Figure 14.1: Total Carbon Column Observing Network (TCCON) in 2015 (Figure courtesy of Dietrich Feist, MPI-BGC, Jena). The station list will be updated on the TCCON wiki and is available from https://tccon-wiki.caltech.edu/Sites

Instruments that are currently accepted in the TCCON are the laboratory type spectrometers Bruker IFS 120HR and Bruker IFS 120HR, with CaF_2 beamsplitters and room-temperature DC-enabled InGaAs detectors. Desired, but not required are DC-enabled Si detectors for the O_2 A-band with dual-beam acquisition. The TCCON imposes the following requirements on the instrument, the acquisition of the interferograms and auxiliary measurements (see also https://tccon-wiki.caltech.edu/index.php?title=Network_Policy/Data_Protocol&highlight=tccon+requirements):

- a minimum spectral range of 4000-9000 cm-1.
- Maximum OPD >= 45 cm with phase resolution of at least 1 cm-1.
- FTS sun tracker pointing with an accuracy of 1 mrad (~0.05º, or 3 arcminutes). This tracker requirement corresponds to an airmass error of 0.2% at 63º SZA, or 0.1% at 45º SZA. This is less strict than the other requirements, because of the practical limitations of available trackers, and may limit overall accuracy. 0.2 mrad, or 0.01º, corresponds to 0.1% airmass error at 80º SZA, and would be ideal. Tracker accuracy should be routinely monitored in one dimension using the solar-telluric shift (S-G shift).
- surface pressure measurements accurate better than 0.3 mbar.
- surface temperature measurements accurate better than 1 K.
- accurate knowledge and reporting of the interferogram ZPD crossing time (within 1 sec).
- laser sampling errors less than 0.00024 of the sample step. This corresponds to a ghost-parent intensity ratio of 0.0001 for parent frequency 4150 cm-1 (NDACC HF filter) and a ghost-parent ratio of 0.00014 for parent frequency of 5970 cm-1 (TCCON ghost filter). The corresponding bias in XCO2 is estimated to be 0.02% or less.
- routine procedures for monitoring instrument line shape (ILS):
    - a line shape monitoring device in the solar beam during all or a continually repeated subset of observations capable of characterizing the modulation efficiency to at least 10% (which implies 0.1% O2 column).
    - monthly ILS retrieval from HCl cell spectra acquired with the tungsten lamp source and analysed with LINEFIT code using the TCCON ILS parameterisation. A SNR of ~2500 is recommended for ILS retrieval from cell spectra, and required for manned sites. A relaxed SNR criteria of ~1300 (typically achieved with ~20 scans) is acceptable for container deployments with limited duration lamp operation.
- criteria for optical alignment, expressed in terms of ME and phase error, to be determined
    - Provisional: The ME shall vary by less than 5% over the 0 to 45 cm OPD, and shall be known to better than 2%.

The Fourier-Transform as well as the retrieval is done with the standardized software package, including a telluric and solar line list (Wunch et al., 2015). The retrieval is done by the individual groups. Before releasing the final TCCON data all retrievals are checked by CALTECH for potential

problems (Wunch et al., 2015). The final TCCON data includes a correction to the WMO standards. This correction is needed due to deficiencies in the spectroscopic data used for the retrieval. The correction factor is obtained from vertical resolved in situ measurements (aircraft or aircore) at TCCON sites. It is important to note that the applied correction factor is the same for all stations. The vertical resolved in situ measurements also allow quantifying the station-to-station bias. A description about the comparisons to vertical resolved in situ measurements as well as an error budget calculation is given in a report by Wunch et al (2015).

Within the EU-project ICOS-INWIRE rapid delivery data (RD-TCCON) from four TCCON sites, including Ny Alesund (Spitsbergen), Trainou (France), Bialystok (Poland) and Reunion (France) was made available one month after the measurement using an automated processing and data transfer. Currently RD-TCCON data from three sites (Trainou, Bialystok, Reunion) is available one month after the measurement for the CAMS84 project. Since other stations are currently not providing RD-TCCON data they are discarded from the validation in CAMS84. However, if RD-TCCON data will become available from other sites over the course of the project, these stations will be included. The RD-TCCON data is processed using the tools provided by the TCCON and contains the automated TCCON quality checks. However, it lacks the final manual quality check. The RD-TCCON data has its own data policy available from the ICOS-ATC.

For the validation reports the RD-TCCON data will be used. Since the RD-TCCON data is processed with the TCCON software and contains the automated TCCON quality checks, the error estimates do not differ from the ones of the final TCCON data, which is described in Wunch et al (2015). However, the RD-TCCON data could be impacted by certain malfunctions of the instrument or the retrieval. An example of an instrumental malfunction would be a misalignment due to an external impact and in case of the retrieval reading a wrong input (e.g. pressure temperature profile). These errors are excluded in the final TCCON data by a thorough manual check of the data. The quantification of these errors is not possible. Usually they are obvious by discontinuities in the time series. Hence if discontinuities in the data exist, this will be discussed in the validation reports.

15 ICOS CO_2/CH_4 surface observations

On November 2015, the European Commission has officially established the Integrated Carbon Observation System (ICOS ERIC). The ICOS European Research Infrastructure Consortium has been established with eight founding members: Belgium, France, Germany, Italy, Netherlands, Norway, Sweden and Finland, which is the ICOS ERIC hosting country, as well as Switzerland which currently has an observer country status.

ICOS is a distributed research infrastructure that provides harmonized European-wide measurements on carbon cycle, on greenhouse gas emissions and on atmospheric concentrations of greenhouse gases. The ICOS RI integrates atmosphere, ecosystem and ocean greenhouse gas monitoring networks in order to provide the observational basis for a full European carbon balance and its trends. Standardized measurements are carried out throughout Europe at tall atmospheric towers and ecosystem sites from the Artic to the Mediterranean, as well as on ocean platforms and vessels covering the North Atlantic, the Mediterranean Sea and the Baltic Sea. Each network is coordinated by its Thematic Centre responsible for data integration and processing, centralized quality control, network training and data transmission. The Atmosphere Thematic Centre (ATC) is based in at LSCE, France.

The stations will have to go through a labelling process, which started in January 2016. So far 25 atmospheric stations (figure 15.1) have applied to be part to ICOS. Pending the labelling of the stations we will use the CO2 and CH4 time series from 15 atmospheric stations that are part of the French monitoring network SNO-RAMCES/ICOS (figure 15.2). Nine stations are located in Western Europe, seven of which in France. Five stations are located in the tropics, and one remote station in the sub Antarctic Indian Ocean. In terms of categories of stations, we can consider six coastal sites (MHD, BIS, STD, FKL, ERS, GUY), four mountain sites (PUY, PDM, RUN, CHC), three tall towers (TRN, OPE, OHP) and one remote site (AMS).

The protocols of the measurements and data processing are consistent with the ICOS specifications. So far all the measurements are done using cavity ring-down spectroscopy (CRDS) analysers (Yver et al., 2015). Each instrument must be regularly (at least once a month) calibrated against reference gases linked to the WMO scales. In addition two target gases are used for the quality control of the dataset and uncertainty assessment. The objective of the ICOS program is to reach the compatibility of measurements recommended by WMO: ±0.1 ppm for CO2 and ±2 ppb for CH4 (WMO/GAW report N°213, 2013).

The dataset have been processed with a standardized algorithm (Hazan et al., 2016). After an automatic check of several parameters, the time series are validated by the station PIs within a three months period after the data acquisition. The model/observation comparison is based on hourly means, without any data selection to separate for example the influence of local from larger scale emissions. The station is compared with the closest grid location of the model. In the horizontal no interpolation is done. For some coastal stations, like Finokalia, we will have to look more closely since the model data are overestimating the CO2 concentrations by about 14 ppm (Fig.12.3). In the vertical the observations are compared to the data extracted at the same elevation

Figure 15.1. Map of the 25 atmospheric stations that have applied to ICOS in January 2016.

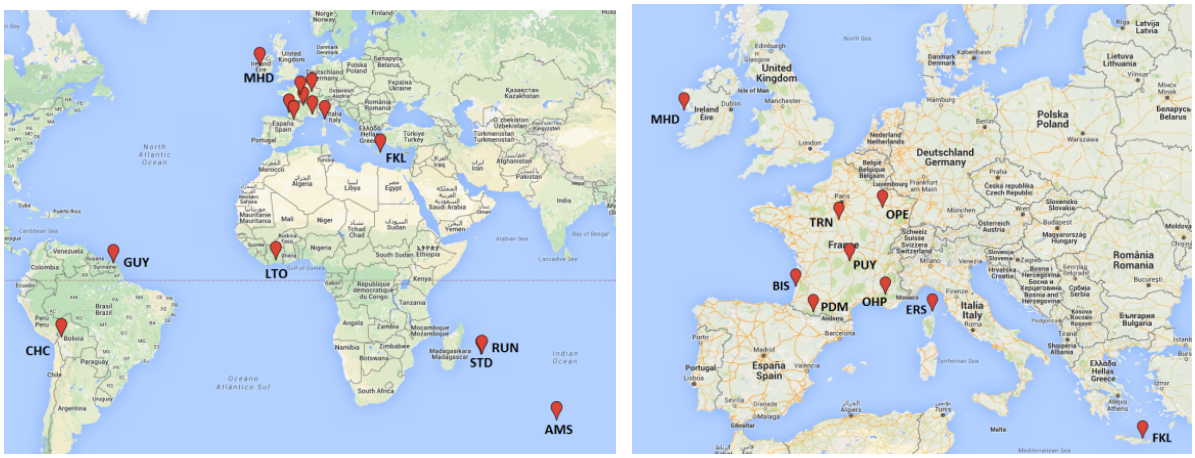

Figure 15.2. Maps of the 15 RAMCES/ICOS surface stations used for the validation in the interim phase.

above the surface, and at the real altitude above sea level. The latter improves the comparability with observations, especially at mountain stations as shown on figure 15.3.

Consequently by default we will use the model data extracted at the sea level altitude of the monitoring site, except if the model altitude of the grid cell corresponding to the location of the site is higher than the station altitude. At the moment the measurement errors are negligible compared to the representativeness error. Our priority will be to improve the comparability of observations with model by filtering out of the observed time series the periods which are strongly influenced by local processes. This selection will be based on the period of the day, and the hourly standard deviation of observations.

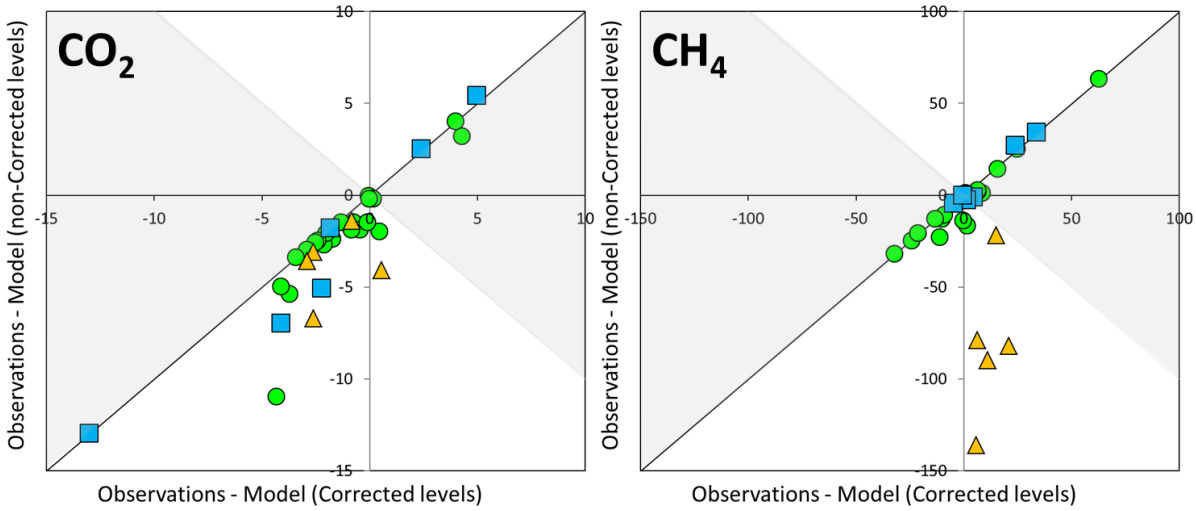

Figure 15.3.Comparisons of the mean CO2 and CH4 differences between observation and forecasts at surface stations (Jan-Sep.2015) when using the non-corrected or corrected vertical levels in the model. Sites are classifies as marine/coastal (blue squares), mountain (orange triangles) or continental (green circles). The grey areas show the cases when the non-corrected version provides better results and the white areas cases when the corrected version is better.

16 Acknowledgements

We wish to acknowledge the provision of NRT GAW observational data by: Institute of Atmospheric Sciences and Climate (ISAC) of the Italian National Research Council (CNR), South African Weather Service, National Centre for Atmospheric Science (NCAS, Cape Verde), National Air Pollution Monitoring Network (NABEL) (Federal Office for the Environment FOEN and Swiss Federal Laboratories for Materials Testing and Research EMPA), Atmospheric Environment Division Global Environment and Marine Department Japan Meteorological Agency, Chinese Academy of Meteorological Sciences (CAMS), Alfred Wegener Institut, Umweltbundesamt (Austria), National Meteorological Service (Argentina), Umweltbundesamt (UBA, Germany)

We are grateful to the numerous operators of the Aeronet network and to the central data processing facility at NASA Goddard Space Flight Center for providing the NRT sun photometer data, and especially Ilya Slutker and Brent Holben for sending the data.

We wish to acknowledge the provision of ozone sonde data by the World Ozone and Ultraviolet Radiation Data Centre established at EC in Toronto (http://woudc.org), by the Data Host Facility of the Network for the Detection of Atmospheric Composition Change established at NOAA (http://ndacc.org), by the Norwegian Institute for Air Research (http://nilu.no) and by the National Aeronautics and Space Administration (https://www.nasa.gov).

We wish to thank the NDACC investigators for the provision of observations at Ny Alesund, Bern, Jungfraujoch, Izaña, Xianghe, Harestua, Reunion Maido, Uccle, Hohenpeissen, Mauna Loa, Lauder and Haute Provence.

The authors acknowledge the NOAA Earth System Research Laboratory (ESRL) Global Monitoring Division (GMD) for the provision of ground based ozone concentrations.

The MOPITT CO data were obtained from the NASA Langley Research Center ASDC. We acknowledge the LATMOS IASI group for providing IASI CO data.

SCIAMACHY lv1 radiances were provided to IUP by ESA through DLR/DFD.

We acknowledge the University of Saskatchewan, Canada for providing the OSIRIS (http://osirus.usask.ca/) observations data and the National Aeronautics and Space Administration (NASA), USA for OMPS (http://npp.gsfc.nasa.gov/omps.html).

We thank the Canadian Space Agency and ACE science team for providing level 2 data retrieved from ACE-FTS on the Canadian satellite SCISAT-1.

The acknowledgements for the TCCON sites included in the CAMS84 validation will be updated on the TCCON wiki and are available from the TCCON data use policy, available from https://tccon-wiki.caltech.edu/Network_Policy/Data_Use_Policy.

We acknowledge the provision of CO_2/CH_4 data from SNO-RAMCES/ICOS network coordinated by LSCE/OVSQ (CEA-CNRS-UVSQ, Université Paris-Saclay), as well as Laboratorio de Física de la Atmósfera (UMSA, Bolivia), Environmental Chemical Processes Laboratory (ECPL/UoC, Greece), Station Géophysique de LAMTO, Ivory Coast), C-CAPS/NUIG/EPA (Ireland), BIRA-IASB (Belgium) and

the following research institutes in France: LaMP/OPGC, P2OA/LA/OMP, OPE/ANDRA, OHP/PYTHEAS, OPAR/LACY/OSUR, UMR EcoFoG, IPEV, IRD

17 References

Adams, C., Strong, K., Batchelor, R. L., Bernath, P. F., et al.: Validation of ACE and OSIRIS ozone and NO 2 measurements using ground-based instruments at 80 ◦ N, Atmos. Meas. Tech., 5, 927–953, doi:10.5194/amt-5-927-2012, 2012.

Adams, C., Bourassa, A. E., Sofieva, V., Froidevaux, L., McLinden, C. A., Hubert, D., Lambert, J.-C., Sioris, C. E., and Degenstein, D. A.: Assessment of Odin-OSIRIS ozone measurements from 2001 to the present using MLS, GOMOS, and ozonesondes, Atmos. Meas. Tech., 7, 49-64, doi:10.5194/amt-7-49-2014, 2014.

Barreto, Á., Cuevas, E., Granados-Muñoz, M.-J., Alados-Arboledas, L., Romero, P. M., Gröbner, J., Kouremeti, N., Almansa, A. F., Stone, T., Toledano, C., Román, R., Sorokin, M., Holben, B., Canini, M., and Yela, M.: The new sun-sky-lunar Cimel CE318-T multiband photometer – a comprehensive performance evaluation, Atmos. Meas. Tech., 9, 631-654, doi:10.5194/amt-9-631-2016, 2016.

Basart, S., Pérez García-Pando, C., Cuevas, E., Baldasano Recio, J. M., & Gobbi, P. (2009). Aerosol characterization in Northern Africa, Northeastern Atlantic, Mediterranean basin and Middle East from direct-sun AERONET observations. Atmospheric chemistry and physics, 9(21), 8265-8282.

Bernath, P. F., McElroy, C. T., Abrams, et al.: Atmospheric Chemistry Experiment (ACE): Mission overview, Geophys. Res. Lett., 32, L15S01, doi:10.1029/2005GL022386, 2005.

Boone, C.D., Nassar, R., Walker, K. A., Rochon, Y., McLeod, S.D., Rinsland, C. P., and Bernath, P. F.: Retrievals for the atmospheric chemistry experiment Fourier-transform spectrometer, Appl. Optics IP, 44, 7218–7231, doi:10.1364/AO.44.007218, 2005.

Brewer, A. and J. Milford (1960), The Oxford Kew ozonesonde, Proc. Roy. Soc.London, Ser. A, 256, 470, 1960.

Boucher, O., Anderson, T.L.. General circulation model assessment of the sensitivity of direct climate forcing by anthropogenic sulfate aerosols to aerosol size and chemistry. Journal of Geophysical Research: Atmospheres 1995;100(D12):26117-26134. Köpke, P., Hess, M., Schult, I., Shettle, E.. Global aerosol data set. Max-Planck-Institut für Meteorologie Hamburg, Germany, 1997.

Bovensmann, H., Burrows, J. P., Buchwitz, M., Frerick, J., Noël, S., Rozanov, V. V., Chance, K. V. and Goede, a. P. H.: SCIAMACHY: Mission Objectives and Measurement Modes, J. Atmos. Sci., 56(2), 127–150, doi:10.1175/1520-0469(1999)056<0127:SMOAMM>2.0.CO;2, 1999.

Clémer, K., Van Roozendael, M., Fayt, C., Hendrick, F., Hermans, C., Pinardi, G., Spurr, R., Wang, P., and De Mazière, M.: Multiple wavelength retrieval of tropospheric aerosol optical properties from MAXDOAS measurements in Beijing, Atmos. Meas. Tech., 3, 863-878, 2010.

Clerbaux C., A. Boynard, L. Clarisse, M. George, J. Hadji-Lazaro, H. Herbin, D. Hurtmans, M. Pommier, A. Razavi, S. Turquety, C. Wespes, and P.-F. Coheur, Monitoring of atmospheric composition using the thermal infrared IASI/MetOp sounder, Atmos. Chem. Phys., 2009.

Christensen, J.H., Brandt, J., Frohn, L.M. and Skov, H., Modelling of mercury with the Danish Eulerian Hemispheric Model, Atm. Chem. Phys. 4, 2251-2257, 2004.

Connor, B. J., Siskind, D. E., Tsou, J. J., Parrish, A., and Remsberg, E. E.: Ground-based microwave observations of ozone in the upper stratosphere and mesosphere, J. Geophys. Res., 99 (D8), 16,757-16,770, 1994.

Cuevas, E., Camino, C., Benedetti, A., Basart, S., Terradellas, E.,Baldasano, J. M., Morcrette, J. J., Marticorena, B., Goloub,P., Mortier, A., Berjón, A., Hernández, Y., Gil-Ojeda, M.,and Schulz, M.: The MACC-II 2007–2008

reanalysis: atmospheric dust evaluation and characterization over northern Africa and the Middle East, Atmos. Chem. Phys., 15, 3991–4024, doi:10.5194/acp-15-3991-2015, 2015.

Deeter, M. N., Emmons, L. K., Edwards, D. P., Gille, J. C., and Drummond, J. R.: Vertical resolution and information content of CO profiles retrieved by MOPITT, Geophys. Res. Lett., 31, L15112, doi:10.1029/2004GL020235, 2004.

Deeter, M. N., et al. (2010), The MOPITT version 4 CO product: Algorithm enhancements, validation, and long-term stability, J. Geophys. Res., 115, D07306, doi:10.1029/2009JD013005.

Deeter M. N., Martinez-Alonso S., Edwards D. P., Emmons L. K., Gille J. C., Worden H. M., Pittman J. V., Daube B. C., Wofsy S. C.: Validation of MOPITT Version 5 thermal-infrared, near-infrared, and multispectral carbon monoxide profile retrievals for 2000–2011, J. Geoph. Res., 118, 12, 2013.

Deeter M. N., Martinez-Alonso S., Edwards D. P., Emmons L. K., Gille J. C., Worden H. M., Sweeney C., Pittman J. V., Daube B. C., and Wofsy S. C.: The MOPITT Version 6 product: algorithm enhancements and validation, Atmos. Meas. Tech, 7, 3623-3632, 2014

de Mazière, M., et al., D8.1 NORS Validation server user requirements document, available as NORS deliverable at http://nors.aeronomie.be/, 2012

de Mazière, M., etal., D4.2 NORS Data user guide, 2013, available as NORS deliverable at http://nors.aeronomie.be/, 2013

Deshler, T., J.L. Mercer, H.G.J. Smit, R. Stubi, G. Levrat, B.J. Johnson, S.J. Oltmans, R. Kivi, A.M. Thompson, J. Witte, J. Davies, F.J. Schmidlin, G. Brothers, T. Sasaki (2008) Atmospheric comparison of electrochemical cell ozonesondes from different maufacturers, and with different cathode solution strengths: The Balloon Experiment on Standards for Ozonsondes. J. Geophys. Res.113, D04307, doi:10.1029/2007JD008975

Dupuy, E., et al.: Validation of ozone measurements from the Atmospheric Chemistry Experiment (ACE), Atmos. Chem. Phys., 9, 287-343, doi:10.5194/acp-9-287-2009, 2009.

Eck, T., Holben, B., Reid, J. S., Dubovik, O., Smirnov, A.,O'Neill, N. T., Slutsker, I., and Kinne, S.: Wavelength dependence of the optical depth of biomass burning urban and desert dust aerosols, J. Geophys. Res., 104, 31333–31349, doi:10.1029/1999JD900923, 1999.

Emmons, L. K., D. P. Edwards, M. N. Deeter, J. C. Gille, T. Campos, P. Nédélec, P. Novelli, and G. Sachse, Measurements of Pollution In The Troposphere (MOPITT) validation through 2006, Atmos. Chem. Phys., 9, 1795-1803, 2009.

Engeln, Axel von, and João Teixeira, A Planetary Boundary Layer Height Climatology Derived from ECMWF Reanalysis Data, Journal of Climate 2013 26:17, 6575-6590, 2013.

Eskes, H. J., and Boersma, K. F.: Averaging kernels for DOAS total-column satellite retrievals, Atmos. Chem. Phys., 3, 1285–1291, 2003.

Eskes, H., Huijnen, V., Arola, A., Benedictow, A., Blechschmidt, A.-M., Botek, E., Boucher, O., Bouarar, I., Chabrillat, S., Cuevas, E., Engelen, R., Flentje, H., Gaudel, A., Griesfeller, J., Jones, L., Kapsomenakis, J., Katragkou, E., Kinne, S., Langerock, B., Razinger, M., Richter, A., Schultz, M., Schulz, M., Sudarchikova, N., Thouret, V., Vrekoussis, M., Wagner, A., and Zerefos, C.: Validation of reactive gases and aerosols in the MACC global analysis and forecast system, Geosci. Model Dev., 8, 3523-3543, doi:10.5194/gmd-8-3523-2015, 2015.

Frieß U., Monks, P.S., Remedios, J.J., Rozanov, A., Sinreich, R., Wagner, T. and Platt, U.: MAX- DOAS O4 measurements: A new technique to derive information on atmospheric aerosols: 2. Modeling studies, J. Geophys. Res. 111, D14203, doi:10.1029/2005JD006618, 2006.

George M., C. Clerbaux, D. Hurtmans, S. Turquety, P.-F. Coheur, M. Pommier, J. Hadji-Lazaro, D. P. Edwards, H. Worden, M. Luo, C. Rinsland, and W. McMillan: Carbon monoxide distributions from the IASI/METOP mission: evaluation with other space-borne remote sensors, Atmos. Chem. Phys., 9, 8317-8330, 2009.

Gielen, C., Van Roozendael, M., Hendrick, F., Pinardi, G., Vlemmix, T., De Bock, V., De Backer, H., Fayt, C., Hermans, C., Gillotay, D., and Wang, P.: A simple and versatile cloud-screening method for MAX-DOAS retrievals, Atmos. Meas. Tech., 7, 3509-3527, doi:10.5194/amt-7-3509-2014, 2014.

Godin, S., G. Mégie and J. Pelon, Geophys. Res. Lett., 1989, 16(16), 547–550. H. Nakane, N. Sugimoto, S. Hayashida, Y. Sasano and I. Matsui, Five years lidar observation of vertical profiles of stratospheric ozone at NIES, Tsukuba (36N, 140E), Proc. 17th ILRC, Sendai, Japan, 1994.

Haeffelin, M., Angelini, F., Morille, Y., Martucci, G., O'Dowd, C. D., Xueref-Rémy, I., Wastine, B., Frey, S., and Sauvage, L.: Eval- uation of mixing depth retrievals from automatic profiling li- dars and ceilometers inview of future integrated networks in Eu- rope, Bound.-Lay. Meteorol., 143, 49–75, doi:10.1007/s10546- 011-9643-z, 2012.

Hazan, L., J. Tarniewicz, M. Ramonet, O. Laurent, A. Abbaris: Automatic processing of atmospheric CO_2 and CH_4 mole fractions at the ICOS Atmospheric Thematic Center, Submitted to Atmos. Meas. Tech.,2016.

Heese, B., Flentje, H., Althausen, D., Ansmann, A., and Frey, S.: Ceilometer lidar comparison: backscatter 5 coefficient retrieval and signal-to-noise ratio determination, Atmos. Meas. Tech., 3, 1763–1770, doi:10.5194/amt-3-1763-2010, 2010.

Heidam, N.Z., Christensen, J.H., Skov, H., Wåhlin, P., Monitoring and modelling of the atmospheric Environment in Greenland. A review., Sci. Total Environ., 331 No. 1-3, 5-28, 2004.

Hocke, K.: Homogenisation of the ozone series of the microwave radiometers SOMORA and GROMOS, IAP Research Report, No. 2007-04-MW, Institut für angewandte Physik, Universität Bern, 2007.

Holben, B. N., Eck, T. F., Slutsker, I., Tanré, D., Buis, J. P., Setzer, A., Vermote, E., Reagan, J. A.,

Kaufman, Y. J., Nakajima, T., Lavenu, F., Jankowiak, I., and Smirnov A.: AERONET – a federated instrument network and data archive for aerosol characterization, Remote Sens. Environ., 66, 1–16, 5529, 5533, 5537, 5544, 1998.

Hurtmans D., Coheur P.-F., Wespes C., Clarisse L., Scharf O., Clerbaux C., Hadji-Lazaro J., George M., Turquety S.: FORLI radiative transfer and retrieval code for IASI, J. Quantitative Spectroscopy and Radiative Transfer, 113, 11, 2012.

ISSI, 2012: Schneider, Matthias, Philippe Demoulin, Ralf Sussmann, and Justus Notholt, Fourier Transform Infrared Spectrometry, Chapter 6 in Monitoring Atmospheric Water Vapour, Ground-Based Remote Sensing and In-situ Methods, ISSI Scientific Report Series, Vol. No. 10 (Editor Niklaus Kämpfer), Springer, DOI 10.1007/978-1-4614-3909-7, 2012, ISBN 978-1-4614-3908-0, 2013.

Jaross, G., G. Chen, M. Kowitt, J. Warner, P. Xu, T. Kelly, M. Linda, and D. Flittner [2012],Suomi NPP OMPS Limb Profiler initial sensor performance assessment, Proc. SPIE,8528, doi:10.1117/12.979627.

Jaross, G., Bhartia, P.K., Chen, G., Kowitt, M., Haken, M., Chen, Z., Xu, Ph., Warner, J., Kelly, T. : OMPS Limb Profiler instrument performance assessment, J. Geophys. Res. Atmos 119, 2169-8996, 2014.

Kämpfer, N.: Monitoring Atmospheric Water Vapour: Ground-Based Remote Sensing and In-situ Methods, ed.: Niklaus Kämpfer, vol.: 10, series: ISSI Scientific Report Series, Springer New York, http://dx.doi.org/10.1007/978-1-4614-3909-7, 2012, ISBN 978-1-4614-3908-0, 2013.

Kobayashi, J. and Y. Toyama: On various methods of measuring the vertical distribution of atmospheric ozone (III) - Carbon iodine type chemical ozonesonde-. Pap. Met. Geophys., 17, 113-126, 1966.

Komhyr, W.D.: Electrochemical concentration cells for gas analysis, Ann.Geoph., 25, 203-210, 1969.

Kramarova, N. A., Nash, E. R., Newman, P. A., Bhartia, P. K., McPeters, R. D., Rault, D. F., Seftor, C. J., Xu, P. Q., and Labow, G. J.: Measuring the Antarctic ozone hole with the new Ozone Mapping and Profiler Suite (OMPS), Atmos. Chem. Phys., 14, 2353-2361, doi:10.5194/acp-14-2353-2014, 2014.

Lambert, J.-C., Atmospheric Service Validation Protocol, Version 2, 28 May 2013, MACC-II document MACCII_MAN_DEL_D153.1_20130528_Lambert_V2.pdf .

Lefever, K.; van der R., A; Baier, F.; Christophe, Y.; Errera, Q.; Eskes, H.; Flemming, J.; Inness, A.; Jones, L.; Lambert, J.-C.; Langerock, B.; Schultz, M. G.; Stein, O.; Wagner, A. & Chabrillat, S.: Copernicus stratospheric ozone service, 2009--2012: validation, system intercomparison and roles of input data sets. Atmos. Chem. Phys., 15 , 2269-2293, doi: 10.5194/acp-15-2269-2015, 2015.

Langerock, B., De Mazière, M., Hendrick, F., Vigouroux, C., Desmet, F., Dils, B., and Niemeijer, S.: Description of algorithms for co-locating and comparing gridded model data with remote-sensing observations, Geosci. Model Dev., 8, pp 911-921, doi:10.5194/gmd-8-911-2015, 2015.

Logan, J., An analysis of ozonesonde data for the troposphere: Recommendations for testing 3-D models and development of a gridded climatology for tropospheric ozone, J. Geophys.Res, 104, pp. 16,115-16,149, 1999.

Marenco, A., V. Thouret, P. Nédélec, H. Smit, M. Helten, D. Kley, F. Karcher, P. Simon, K. Law, J. Pyle, G. Poschmann, R. Von Wrede, C. Hume and T. Cook, Measurement of ozone and water vapor by Airbus in-service aircraft: The MOZAIC airborne program, An overview, J. Geophys. Res., 103, 25,631-25,642, 1998.

McGee, T.J., M. Gross, R. Ferrare, W. S. Heaps and U. N. Singh, Geophys. Res. Lett., 1993, 20, 955– 958.

Morcrette, J.J., Beljaars, A., Benedetti, A., Jones, L., Boucher, O., Sea-salt and dust aerosols in the ECMWF IFS model. Geophysical Research Letters 2008; 35(24). L24813.

Morcrette, J.J., Boucher, O., Jones, L., Salmond, D., Bechtold, P., Beljaars, A., Benedetti, A., Bonet, A., Kaiser, J.W., Razinger, M., Schulz, M., Serrar, S., Simmons, A.J., So_ev, M., Suttie, M., Tompkins, A.M., Untch, A., Aerosol analysis and forecast in the european centre for medium range weather forecasts integrated forecast system: Forward modeling. Journal of Geophysical Research: Atmospheres 2009; 114(D6), D06206.

Munro, R., Lang, R., Klaes, D., Poli, G., Retscher, C., Lindstrot, R., Huckle, R., Lacan, A., Grzegorski, M., Holdak, A., Kokhanovsky, A., Livschitz, J. and Eisinger, M.: The GOME-2 instrument on the Metop series of satellites: instrument design, calibration, and level 1 data processing – an overview, Atmos. Meas. Tech., 9(3), 1279–1301, doi:10.5194/amt-9-1279-2016, 2016.

Nédélec P., Blot R., Boulanger D., Athier G., Cousin J-M., Gautron B., Petzold A., Volz-Thomas A. and Thouret V., Instrumentation on commercial aircraft for monitoring the atmospheric composition on a global scale: the IAGOS system, technical overview of ozone and carbon monoxide measurements, MOZAIC-IAGOS special issue, Tellus B 2015, 67, 27791, http://dx.doi.org/10.3402./tellusb.v67.27791

O'Dowd, C.D., Lowe, J.A., Smith, M.H., Davison, B., Hewitt, C.N., Harrison, R.M.. Biogenic sulphur emissions and inferred non-sea-salt sulphate cloud condensation nuclei in and around antarctica. Journal of Geophysical Research: Atmospheres 1997; 102(D11):12839-12854.

Oltmans, S.J. and Komhyr, W.D. (1986). Surface ozone distributions and variations from 1973 – 1984 measurements at the NOAA geophysical monitoring for climatic change baseline observatories.. Journal of Geophysical Research 91: doi: 10.1029/JD091iD04p05229. issn: 0148-0227

Oltmans, SJ and Levy II, H, Surface ozone measurements from a global network, Atmos. Environ., 28, 9-24, 1994.

O'Neill, N. T., Eck, T. F., Holben, B. N., Smirnov, A., Dubovik, O., Royer, A.: Bi-modal size distribution influences on the variation of Angstrom derivatives in spectral and optical depth space, J. Geophys. Res., vol. 106, 9787-9806, 2001.

O'Neill, N. T., Eck, T. F., Smirnov, A., Holben, B. N. and Thulasiraman, S., Spectral discrimination of coarse and fine mode optical depth, J. Geophys. Res., 108, 4559, 2003.

Peter, R.: The Ground-based Millimeter-wave Ozone Spectrometer - GROMOS, IAP Research Report, No. 1997-13, Institut für angewandte Physik, Universitaät Bern, 1997.

Petzold A., V. Thouret, C. Gerbig, A. Zahn, C. A.M. Brenninkmeijer, M. Gallagher, M. Hermann, M. Pontaud, H. Ziereis, D. Boulanger, J. Marshall, P. Nédélec, H. G.J. Smit, U. Friess, J.-M. Flaud, A. Wahner, J.-P. Cammas, A. Volz-Thomas, Global-scale atmosphere monitoring by in-service aircraft current achievements and future prospects of the European Research Infrastructure IAGOS, Tellus B 2015, 67, 28452, http://dx.doi.org/10.3402/tellusb.v67.28452.

Pumphrey, H. C., M. L. Santee, N. J. Livesey, M. J. Schwartz, and W. G. Read: Microwave Limb Sounder observations of biomass-burning products from the Australian bush fires of February 2009, Atmos. Chem. Phys., 11, 6285-6296, 2011

Reddy, M.S., Boucher, O., Bellouin, N., Schulz, M., Balkanski, Y., Dufresne, J.L., Pham, M.. Estimates of global multicomponent aerosol optical depth and direct radiative perturbation in the laboratoire de meteorologie dynamique general circulation model. Journal of Geophysical Research: Atmospheres 2005; 110(D10), D10S16.

Richter, A., Burrows, J. P., Nüss, H., Granier, C. and Niemeier, U.: Increase in tropospheric nitrogen dioxide over China observed from space., Nature, 437(7055), 129–32, doi:10.1038/nature04092, 2005.

*Richter, A., Begoin, M., Hilboll, A., and Burrows, J. P.: An improved NO2 retrieval for the GOME-2 satellite instrument, Atmos. Meas. Tech. , **4**, 1147-1159, doi:10.5194/amt-4-1147-2011, 2011*

Rodgers, C. D.: Inverse Methods for Atmospheric Sounding, Theory and Practice, World Scientific, Singapore, 2000.

Schmid, B., Michalsky, J., Halthore, R., Beauharnois, M., Harisson,L., Livingston, J., Russell, P., Holben, B., Eck, T., and Smirnov, A.: Comparison of aerosol optical depth from four solar radiometers during the fall 1997 ARM intensive observation period, J. Geophys. Res., 26, 2725–2728, 1999.

*Sheese, P. E.; Walker, K. A.; Boone, C. D.; Bernath, P. F.; Froidevaux, L.; Funke, B.; Raspollini, P. & von Clarmann, T.: ACE-FTS ozone, water vapour, nitrous oxide, nitric acid, and carbon monoxide profile comparisons with MIPAS and MLS. J. Quant. Spect. Rad. Transfer, **186**, 63 – 8, doi:10.1016/j.jqsrt.2016.06.026, 2017.*

Skov, H., Hertel, O. Bech Poulsen, M., Christensen, J.H. and Nordstrøm C. The dynamics of gaseous elemental mercury and ozone at Villum Research Station, Station Nord. Under preparation March 2016 for Atmos. Chem. Phys.

Skov, H., Christensen, J., Goodsite, M.E., Heidam, N.Z., Jensen, B., Wåhlin, P. and Geernaert, G., The fate of elemental mercury in Arctic during atmospheric mercury depletion episodes and the load of atmospheric mercury to Arctic, Environ. Sci. Technol. 38, 2373-2382, 2004.

Smit, H.G.J.: Ozonesondes, in Encyclopedia of Atmospheric Sciences, edited by J. Holton, J. Pyle, and J. Curry, pp. 1469-1476, Academic Press, London, 2002.

Smit, H.G.J., W. Straeter, B.J. Johnson, S.J. Oltmans, J. Davies, D.W. Tarasick, B. Hoegger, R. Stubi, F.J. Schmidlin, T. Northam, A.M. Thompson, J.C. Witte, I. Boyd: Assessment of the performance of ECC-ozonesondes under quasi-flight conditions in the environmental simulation chamber: Insights from the Juelich Ozone Sonde Intercomparison Experiment (JOSIE), J. Geophys. Res. 112, D19306, doi:10.1029/2006JD007308, 2007.

Smit, H.G.J.: Quality Assurance and Quality Control for Ozonesonde Measurements in GAW. WMO/GAW No. 201, World Meteorological Organisation, Geneva, 2013.

Seckmeyer G., A. Bais, G. Bernhard, M. Blumthaler, C.R. Booth, K. Lantz, R.L. McKenzie, P. Disterhoft, and A. Webb (2006), Instruments to measure solar ultraviolet radiation Part 2: Broadband instruments measuring erythemally weighted solar irradiance. Draft available at: http://www.wmo.ch/ web/arep/reports/gaw164_final_draft.pdf, WMO/GAW No. 164 World Meteorological Organisation, Geneva.

Staehelin, J.: Global atmospheric ozone monitoring. WMO Bulletin, Volume 57 (1), Geneva, 2008

Taha, G.; Jaross, G. R.; Bhartia, P. K.: Validation of OMPS LP Ozone Profiles Version 2.0 with MLS, Ozone Sondes and Lidar Measurements, American Geophysical Union, Fall Meeting 2014, abstract #A33J-3322, 2014.

Tegtmeier, S.; Hegglin, M. I. et al. : SPARC Data Initiative: A comparison of ozone climatologies from international satellite limb sounders. J. Geophys. Res.: Atmos., 118, 12,229-12,247, doi:10.1002/2013JD019877, 2013.

Teschke, G. and K. Poenitz, 2010: On the retrieval of aerosol (mixing) layer heights on the basis of ceilometer data. International Symposium for the Advancement of Boundary Layer Remote Sensing. 28.-30.06.2010. Paris.

Vrekoussis, M., Wittrock, F., Richter, A. and Burrows, J. P.: GOME-2 observations of oxygenated VOCs: what can we learn from the ratio glyoxal to formaldehyde on a global scale?, Atmos. Chem. Phys., 10(21), 10145–10160, doi:10.5194/acp-10-10145-2010, 2010.

Walker, K., Jones, S., Sheese, P., Boone, C. and P. Bernath: ACE – FTS Atmospheric Chemistry Experiment. Data usage guide and file format description for ACE-FTS level 2 data version 3.5/3.6 ASCII format. Doc. ACE-SOC 0030, https://databace.scisat.ca/level2/ace_v3.5_v3.6/ACE-SOC-0030-1A-ACE-FTS_ascii_data_usage_and_fileformat_for_v3.5-3.6-16Jan2017.pdf , 16 January 2017

Wang, P., P. Stammes, R. van der A, G. Pinardi, M. van Roozendael, FRESCO+: an improved O2 A-band cloud retrieval algorithm for tropospheric trace gas retrievals, Atmospheric Chemistry and Physics, 8, 6565-6576, 2008.

Wiegner, M. and Geiß, A.: Aerosol profiling with the Jenoptik ceilometer CHM15kx, Atmos. Meas. Tech., 5, 1953–1964, doi:10.5194/amt-5-1953-2012, 2012.

Wittrock, F., A. Richter, H. Oetjen, J. P. Burrows, M. Kanakidou, S. Myriokefalitakis, R. Volkamer, S. Beirle, U. Platt, and T. Wagner, Simultaneous global observations of glyoxal and formaldehyde from space, Geophys. Res. Lett., 33, L16804, doi:10.1029/2006GL026310, 2006.

WMO (2010), Guidelines for the Measurement of Atmospheric Carbon Monoxide, GAW Report No. 192, World Meteorological Organization, Geneva, Switzerland, 2010.

WMO (2013), Guidelines for the Continuous Measurements of Ozone in the Troposphere, GAW Report No. 209, World Meteorological Organization, Geneva, Switzerland, 2013.

WMO/GAW (2013), 17th WMO/IAEA Meeting on Carbon Dioxide, Other Greenhouse Gases and Related Tracers Measurement Techniques, Beijing, China, GAW Report No. 213, 2013.

Wunch, D., Toon, G. C., Wennberg, P. O., Wofsy, S. C., Stephens, B. B., Fischer, M. L., Uchino, O., Abshire, J. B., Bernath, P., Biraud, S. C., Blavier, J.-F. L., Boone, C., Bowman, K. P., Browell, E. V., Campos, T., Connor, B. J., Daube, B. C., Deutscher, N. M., Diao, M., Elkins, J. W., Gerbig, C., Gottlieb, E., Griffith, D. W. T., Hurst, D. F., Jimenez, R., Keppel-Aleks, G., Kort, E. A., Macatangay, R., Machida, T., Matsueda, H., Moore, F., Morino, I., Park, S., Robinson, J., Roehl, C. M., Sawa, Y., Sherlock, V., Sweeney, C., Tanaka, T., and Zondlo, M. A.: Calibration of the Total Carbon Column Observing Network using aircraft profile data, Atmos. Meas. Tech., 3, 1351-1362, doi:10.5194/amt-3-1351-2010, 2010. Available from: http://www.atmos-meas-tech.net/3/1351/2010/.

Wunch D., G.C. Toon, J.-F.L. Blavier, R.A. Washenfelder, J. Notholt, B.J. Connor, D.W.T. Griffith, V. Sherlock, P.O. Wennberg. The Total Carbon Column Observing Network. Phil. Trans. R. Soc. A 369, doi:10.1098/rsta.2010.0240, 2011.

Xu Philippe Q., Pawan K. Bhartia , Glen R. Jaross , Matthew T. DeLand , Jack C. Larsen , Albert Fleig , Daniel Kahn , Tong Zhu , Zhong Chen , Nick Gorkavyi , Jeremy Warner , Mike Linda , Hong Chen , Mark Kowitt , Michael Haken , Peter Hall, Release 2 data products from the Ozone Mapping and Profiler Suite (OMPS) Limb Profiler. Proc. SPIE 9242, Remote Sensing of Clouds and the Atmosphere XIX; and Optics in Atmospheric Propagation and Adaptive Systems XVII, 92420K (October 17, 2014); doi:10.1117/12.2067320.

Yver-Kwok, C., O. Laurent, A. Guemri, C. Philippon, B. Wastine, C.W. Rella, C. Vuillemin, F. Truong, M. Delmotte, V. Kazan, M. Darding, B. Lebègue, C. Kaiser, I. Xueref-Remy, and M. Ramonet: Comprehensive laboratory and field testing of cavity ring-down spectroscopy analyzers measuring H2O, CO2, CH4 and CO, Atmos. Meas. Tech., 8, 3867-3892, 2015

18 Annex: Regions

Figure A2.1 shows the regions used for spatial data-stratification as adopted for CO total and NO_2 tropospheric column evaluation (left) as well as H_2CO tropospheric column evaluation (right). The number of regions is limited to eight, including industrially polluted regions, (tropical) biomass burning region and a polar region. The following regions are defined: Europe (15W–35E, 35N–70N), Fires-Alaska (150W–105W, 55N–70N), Fires-Siberia (100E–140E, 40N–65N), North Africa (15W–45E, 0N–20N), South Africa (15E–45E, 20S–0S), South Asia (50E–95E, 5N–35N), East Asia (100E–142E, 20N–45N), United States (120W–65W, 30N–45N). Figure A2.2 shows the aggregation of ozone sonde profiles, where all profiles within five different latitude bands are combined. Stratospheric evaluations are also aggregated within these five latitude bands.

The rationale behind the use of various regions is dictated by the emissions and chemistry at stake, in combination with available observations. Major anthropogenic and biomass burning emission hotspots emitting CO, NO_2, H_2CO are well visible from the various satellite instruments, while for O_3 this aggregation is constrained by the availability of sounding observations distributed over the globe. In the stratosphere horizontal gradients are generally more smooth.

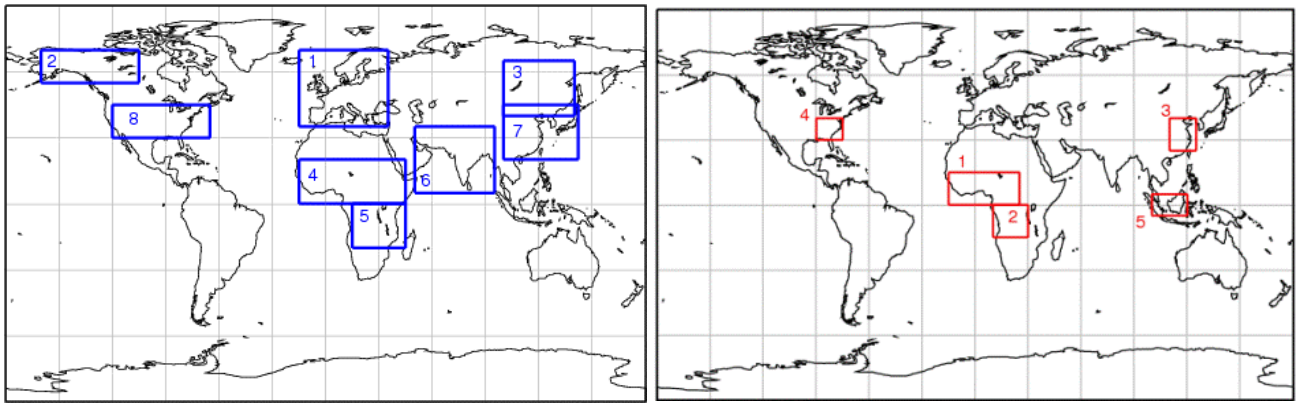

Figure A2.1. (left) Recommended regions for spatial aggregation. (right) Chosen data stratification for HCHO analysis.

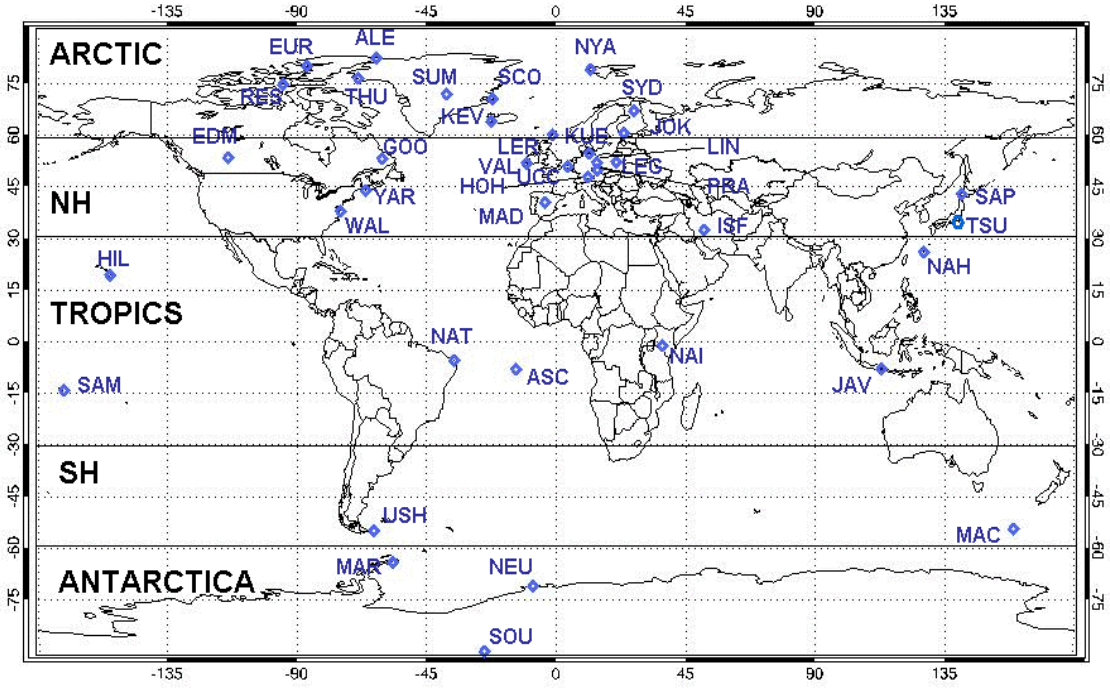

Figure A2.2: Location of the ozone sounding stations and their attribution to the different stratospheric regions

Copernicus Atmosphere Monitoring Service

ECMWF - Shinfield Park, Reading RG2 9AX, UK

Contact: info@copernicus-atmosphere.eu